EARTH PROJECT

(ESF-3763)

"European level Atmospheric Radon Transport: High resolution simulations"

Final Report

Dr. I. López-Coto

(israel.lopez@dfa.uhu.es)

Applied Physics Department at Huelva University
Huelva (Spain)

Huelva, 2012

Abstract

The EARTH project, developed within the framework of the European Science Foundation activity entitled "Tall Tower and Surface Research Network for Verification of Climate Relevant Emissions of Human Origin (TTORCH)", had as principal aim including radon as natural tracer for transport and mixing processes in the WRF-Chem model.

With this in mind, a time dependent radon flux inventory has been evaluated, showing in general a good agreement with previous inventories. Besides, the radon decay process has been included into WRF-GHG model and the time dependent inventory and other 3 static inventories have been coupled to WRF-CHEM-GHG in offline mode using TM3 derived initial and boundary conditions.

In order to validate the simulation system results and evaluate the inventories performances, five 13-days periods have been simulated and the results have been compared against radon concentration measurements from 6 stations showing in general good agreement with overall RMSD of around 1 Bq m^{-3}. Besides, different events of the simulated time-series, during which the simulations indicated especially large deviations from the observations, have been analyzed in detail in order to assess potential reasons for mismatches.

After results of this project, it is possible to assure that including the radon decay process into WRF-CHEM along with the time dependent radon flux inventory and testing the simulations results against radon data time series from experimental measurement stations have been a fundamental first step towards an operational evaluation of model performance with high relevance for estimation of GHG exchange fluxes derived from atmospheric observations.

Keywords: Time dependent radon flux inventory, atmospheric radon observations, atmospheric radon transport simulations, WRF-GHG.

Acknowledgments

The author wishes to sincerely thank to John Moncrieff, Alex Vermeulen, Rebecca Fisher, Ingeborg Levin, Martina Schmidt, Rolf Neubert and Harro Meijer for providing atmospheric radon concentration data and to Thomas Szegvary and Franz Conen for providing their radon flux inventory through the web (http://radon.unibas.ch)

A special mention is required to Dr. Christoph Gerbig, Dr. Ute Karsten, Roberto Kretschmer, Veronika Beck and Thomas Koch for their scientific comments and technical support and the whole Max Plank Institute for Biogeochemistry Jena for the hospitality.

This work has been funded by the European Science Foundation within the framework of the activity entitled "Tall Tower and Surface Research Network for Verification of Climate Relevant Emissions of Human Origin (TTORCH)". Reference code: ESF-3763

1. Introduction

The first step in stabilizing the concentrations of the greenhouse gases (GHG) in our atmosphere is to estimate the emissions of these GHG and its primary sources and sinks. The Kyoto protocol is seen as a first step towards reduction of the emissions of GHG for a better sustainable future and requires that the world countries establish a system (national emission inventories) to quantify their emissions of GHG by different sectors and also their primary sources and sinks. The emission inventories might be inaccurate or incomplete and hence it is important to validate the GHG inventories.

In the other hand, global or regional model used to simulate the behavior of theses gases in the atmosphere rely on several assumptions and simplifications in order to achieve and equilibrium between performance and computational needed. In this sense, the models performance need to be evaluated and verified in a continual way in order to assure the precision and trueness of results as well as associated uncertainties.

The natural radioactive noble gas radon, ^{222}Rn, is a decay product of ^{226}Ra in the long decay chain of ^{238}U. Radon is mostly of terrestrial origin and it is dispersed in the air by atmospheric transport and mixing. Radon is a noble gas (no deposition, washout or chemical reactions), so the only loss mechanism is radioactive decay and thus the residence time of radon in the atmosphere is well known.

Trace gas emissions of GHG originating from large terrestrial systems can be estimated using radon as a marker for emissions from the soil. Thus, continuous ^{222}Rn monitoring allows for estimating regional trace gas fluxes by means of the Radon-Tracer-Method (Schmidt et al., 2001, Gurney et al., 2002; Rodenbeck et al., 2003; Bousquet et al., 2006), if the soil exhalation rate of ^{222}Rn in the catchment area is adequately known. Besides, simulating radon transport is currently one of the best tools for the evaluation of transport schemes in regional to global climate/atmospheric models, (Jacob et al., 1997; Dentener et al., 1999). Nevertheless, the usefulness of this tool is limited to the quality of the emission rate of radon from soil to atmosphere inventories.

Until now, radon inventories have low spatial resolution, and are not dependent on the weather conditions (Rasch et al., 2000; Conen and Robertson, 2002). A more accurate inventory at the European level, has been described in Szegvary et al., (2009) based on experimental correlations between exhalation rate and dose rate of external gamma radiation exposure. It also includes temporal variations in the exhalation rate derived from variations of gamma dose rate. However, the different isotopic composition of soils in Europe limits the applicability of the correlations used in obtaining exhalation, showing areas where predicted exhalation does not correspond to the experimental results (Grossi, et al. 2011)

Recently, the Huelva University (UHU) has developed an inventory of radon emissions into the atmosphere, at European level, with high spatial resolution and dependent on meteorological variables (López-Coto, 2011). This inventory has shown good agreement with both experimental and simulated published results, and it appears as a valuable alternative in order to improve the quality of GHG inventories estimations, and quantitatively evaluate atmospheric transport models and their uncertainties.

With all these ideas in mind, the principal aim of this project is to include the UHU radon flux inventory and the radon decay process into WRF-CHEM model, which represents the state of the art in atmospheric transport and chemical modeling, and to test the behavior of this system under real

conditions by means of comparison between simulation results and experimental radon concentration data from atmospheric network stations. This will serve as starting point for a quantitative validation of the WRF-Chem transport model, and for a more quantitative GHG source estimation.

2. Materials and Methods

In the figure 1, a procedures flowchart is shown. The work structure is divided into three general phases: radon flux inventories adaptation, atmospheric transport model adaptation and system validation.

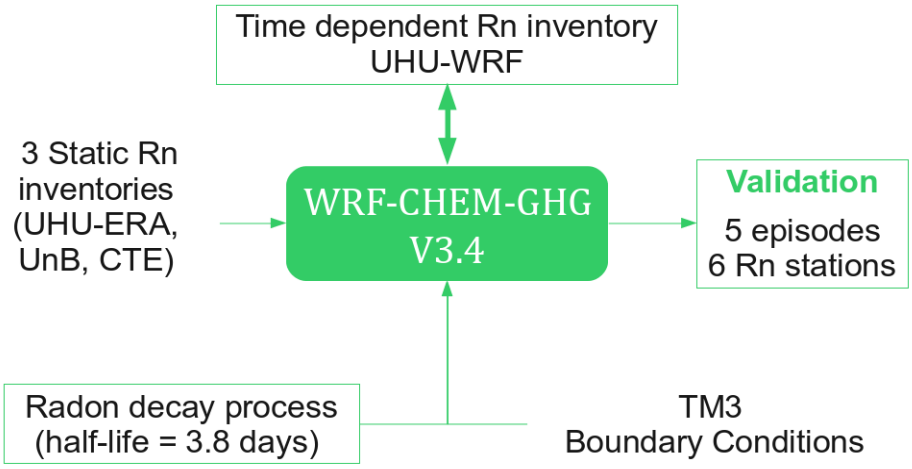

Figure 1. Procedures general flowchart

2.1. Rn fluxes inventories

In this work four radon flux inventories are employed; three of them are static in time and one is calculated in time dependent way from the meteorological conditions. Comparisons of simulated atmospheric radon concentrations resulting from these inventories allows for a first assessment of the performance and of the impact of differences in flux inventories.

2.1.1. Static inventories

a) UHU-ERA

Recently, the Huelva University (UHU) has developed a 40-year retrospective high-resolution European radon flux inventory basing on the fundamental equation of radon transport in porous media, taking into account the dependency of the transport coefficient on temperature and humidity. It also includes a simple model that evaluates the effect of snow cover, (López-Coto, 2011). This model uses geological, geochemical and climatological parameters of the soils with a horizontal resolution of 0.5' (1 km). This

inventory provides us a high resolution radon flux map for each 40 years composed month.

The corresponding month for each simulation period was selected, and the resolution and domain coverage were adapted to the selected European domain.

b) UnB

An statistical approach has been described in Szegvary et al., (2009). It is based on experimental correlations between exhalation rate and dose rate of external gamma radiation exposure. It also includes temporal variations in the exhalation rate derived from variations of gamma dose rate. However, the different isotopic composition of soils in Europe limits the applicability of the correlations used in obtaining exhalation, showing areas where predicted exhalation does not correspond to the experimental results (Grossi, et al. 2011)

The 2006 annual averaged inventory was selected and the resolution and domain coverage were adapted to the selected European domain.

c) CTE

From the European radon flux average value given by UHU-ERA, 30 Bq m^{-2} h^{-1}, a constant in space and time radon flux inventory has been set up.

2.1.2. Dynamic inventory (UHU-WRF)

The dynamic inventory used in this work is a modification of the UHU-ERA inventory code in order to calculate the Radon fluxes in time-dependent mode taking as meteorological input the soil moisture, soil temperature and snow cover directly from WRF simulations in a European domain of 399 x 279 grid cells with a spatial resolution of 10 x 10 km^2 and a temporal resolution of 1 hour.

The theoretical model is based on the fundamental equation of radon transport in porous media, taking into account the dependency of the transport coefficient on temperature and humidity. It also includes a simple model that evaluates the effect of snow cover (López-Coto, 2011).

The numerical solver has been based on the forward difference method and has been written in C++. This code enables the calculation of the radon concentration profile in time dependent mode from the data files directly taken from WRF simulations.

The solver subroutine interpolates variables depending on z, using splines, and calculates the diffusion coefficient for each cell in the soil profile, (dz = 0.03 m). Then, it solves the equation of time-dependent one-dimensional transport in an iterative way with a time step of dt = 30s. After that, the exhalation rate is calculated from the radon concentration soil profile with an input-output frequency of 1 hour.

The initial condition for the radon soil profile is fixed to zero in the model. For this reason, the model includes an algorithm, which allows for calculating a steady state solution in the initial time step, and taking this as initial conditions to the next time step. This method is called “auto spin up method” in the text.

2.2. Atmospheric transport models

The atmospheric transport model employed in this work has been the WRF-CHEM-GHG developed by MPI-BGC. The WRF Greenhouse Gases model (WRF-GHG) is an augmentation of the coupled Weather Research and Forecasting model (WRF) to the Vegetation Photosynthesis and Respiration model (VPRM), WRF-VPRM, which is described in detail in Ahmadov et al. (2007). The main objective of WRF-VPRM is to simulate high-resolution passive tracer transport of carbon dioxide (CO_2). WRF-GHG (Beck et al., 2011) is an extension of WRF-VPRM allowing for passive tracer transport not only for CO_2, but also for methane (CH_4) and carbon monoxide (CO). A further advantage of both WRF-GHG and WRF-VPRM is that initial and boundary conditions can be provided from three-dimensional fields of global simulations of CO_2 , CH_4 and CO.

The WRF model (ARW core) uses fully compressible, non-hydrostatic Eulerian equations on an Arakawa C-staggered grid with conservation of mass, momentum, entropy, and scalars (Skamarock et al., 2008). Tracers are transported online in a passive way, i.e. without any chemical reactions within the framework of the GHG–TRACER package. Therefore all chemical mechanisms besides vertical mixing are turned off if the tracer transport option is used (Ahmadov et al., 2007). Online tracer transport implies that transport is performed simultaneously with the meteorological variables at each time step (Ahmadov et al., 2007). Emissions are added at each time step to the tracer concentration in the lowest model layer. The tracers undergo the advection, boundary layer, and convective mixing as the chemical species. The MYNN2 scheme (Nakanishi and Niino, 2006) was selected as boundary layer parametrization, the Kessler scheme (Kessler, 1969) was selected as Micro-physics parametrization and the Grell-Devenyi scheme (Grell and Devenyi, 2002) was selected as convective scheme. Besides, 41 vertical pressure following levels were set and the ECMWF reanalysis data were used as meteorological inputs.

The radon initial and boundary conditions for WRF-CHEM-GHG model have been obtained from TM3 transport model (Heimann and Körner, 2003) running with a simple radon flux inventory of 1 atom cm^{-2} s^{-1} (75.5 Bq m^{-2} h^{-1}). The TM3 model is a three dimensional Eulerian transport model that solves the continuity equation based on given time-dependent meteorological fields for the surface pressure, wind velocity, air temperature and geopotential. Evaporation fluxes are also needed to calculate the transport by cumulus clouds. These forcing fields may be obtained from an atmospheric general circulation model or from weather model forecast, or from meteorological analysis, for example from NCEP. For a realistic calculation the meteorological fields have to use a time step on the order of hours.

2.3. Rn data and simulated periods

The radon concentration data have been obtained from 6 measurement stations across Europe. Their location and topographic surrounding varies considerably ranging from rooftop stations in cities, to single stations on mountain ridges or coastal borders. Not only the topographic surrounding is complex, but also the geological one, Europe being a continent with very different expected radon exhalation rates.

For its part, Angus, Cabauw, Lutjewad and Gif were using the ANSTO two-filter radon detector (Whittlestone and Zahorowski, 1998) and the Egham station was using a Radon monitor based on the ^{218}Po electro-deposition method developed at University of Heidelberg (Levin et al., 2002)

Table 1. Station locations and sampling height

Station	Latitude	Longitude	Height (masl)
Angus (UK)	56.55	-2.98	313
Cabauw (Netherlands)	51.97	4.93	20
Cabauw (Netherlands)	51.97	4.93	200
Lutjewad (Netherlands)	53.4	6.35	60
Gif-sur-Yvette LSCE (France)	48.71	2.15	180
Egham RHUL (UK)	51.43	-0.56	40

Five simulations periods have been selected between 2007 and 2009 in order to capture the different seasons. Besides, the event duration has been set to 13 days in order to simulate the transport during a time at least 3 times longer than the radon half-life. With this, the selected periods were: 01/05/2007- 14/05/2007, 01/02/2008- 14/02/2008, 01/07/2008- 14/07/2008, 01/12/2008- 14/12/2008, 01/10/2009- 14/10/2009.

2.4 Testing methods

2.4.1 Score evaluation

In general, we are employed the mean difference (BIAS) and the root mean square deviation (RMSD) as score estimators. Besides, we are calculated the differences probability distribution in order to calculate the most probable value (MODE) and other statistical estimators as the percentiles.

$$\Delta_i = x_i - x_i^{Ref} \quad (1)$$

$$BIAS = \frac{1}{N}\sum_{i=1}^{N} \Delta_i \quad (2)$$

$$RMSD = \sqrt{\frac{1}{N}\sum_{i=1}^{N} \Delta_i^2} \quad (3)$$

2.4.2 Radon flux model "spin-up" time

Once the radon flux model was converted to time dependent, two "Spin up time" testing methods were applied:

a) Approach 1: 8 days simulation test with and without auto spin up method

In this approach we are compared the hourly simulation results obtained by means the auto spin up method and the calculations beginning with zero initial condition. Thus, we can get a quantitative estimate about the initialization time required by the radon flux model.

The hourly relative fluxes differences obtained per each cell have been fitted to a first order exponential function in order to calculate the average "half-life" of the initialization time or spin up.

The half-life is defined as the required time to obtain the 50% of the relative differences.

b) Approach 2: 8 days simulation test with sequential initialization of the auto spin up method

This second approach compares the fluxes obtained in the last time step by means of the auto spin up method for eight simulations ending in the same day but using 1 to 8 running days, figure 2. We are taken the eight days simulation as reference for BIAS and RMSD calculation and we are analyzed the evolution with running days.

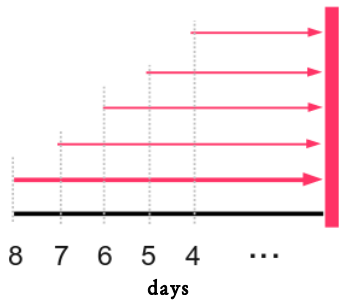

Figure 2. Schematic representation of the "sequential initialization" testing method

2.4.3 Radon fluxes comparison

We compared the radon fluxes predicted by the UHU-ERA, UnB and UHU-WRF inventories for the whole domain during a single simulated episode of 10 days (01/10/2009-10/10/2009). We employed the 40 years averaged November for the UHU-ERA inventory, the 2006 year averaged UnB inventory and the hourly weather dependent UHU-WRF inventory.

The flux differences between them have been calculated and the BIAS and RMSD alongside the probability distribution have been obtained.

2.4.4 Radon concentrations comparison

The simulated radon concentrations time series have been extracted from the WRF output and have been lineally interpolated between model levels in order to match the stations sampling heights. Besides,

the observed radon data have been filtered in order to avoid non numeric values.

The hourly simulated atmospheric radon concentrations obtained using the different inventories have been compared against the observed radon concentration and the hourly differences have been calculated alongside the BIAS, RMSD, MODE, percentiles and the density and cumulated probability distributions.

3. Results

3.1. Radon flux model "spin-up" time

3.1.1 Approach 1

The figure 3.a shows the temporal evolution of the relative differences between the fluxes obtained with and without the auto spin up initialization method for one domain cell and the exponential fit obtained. Besides, the figure 3.b shows the calculated half life probability distribution. The auto spin up solution is taken as reference in this part.

As expected, the relative difference evolution follows a very well defined exponential growth derived from the radon ingrowth in the soil profile. As can be seen in the figure 3.a, the eight days simulation are not enough to reach a relative deviation below 5%. Besides, the average initialization half-life is around 38 h with a standard deviation of 3.6 h. This means that the model initializated with zero initial condition requires around 11 days (seven half-lifes) to reproduce the fluxes obtained with the auto spin up initialization method.

With all of this, it is possible to assure that the auto spin up method is reducing the initialization time from around eleven days to only one hour. This fact has a direct implication in the model operation, since the inclusion of the auto spin up method avoids the need for simulating previous days meteorological fields.

3.1.2 Approach 2

The figure 4.a shows the probability distribution of the relative differences between the fluxes calculated using 1 day and 8 days of meteorological data. Besides, the figure 4.b shows the BIAS and RMSD as functions of running days.

As can be seen, the calculated relative differences BIAS is below 5% in all cases and it quickly decreases with the number of running days. In this period, the BIAS is positive in all cases but this is only by chance because the initial state is depending on the specific meteorological conditions and, in the same way, the final state is depending on the period meteorological history. Thus, we can expect periods with negative BIAS as well.

Besides, the RMSD is around 13% for one running day and it decreases below 5% for two running days. This means the radon flux model working with the auto spin up initialization method requires some time to stabilizing the radon concentration soil profile solution; based on results, we can suggest one or two days of stabilizing time.

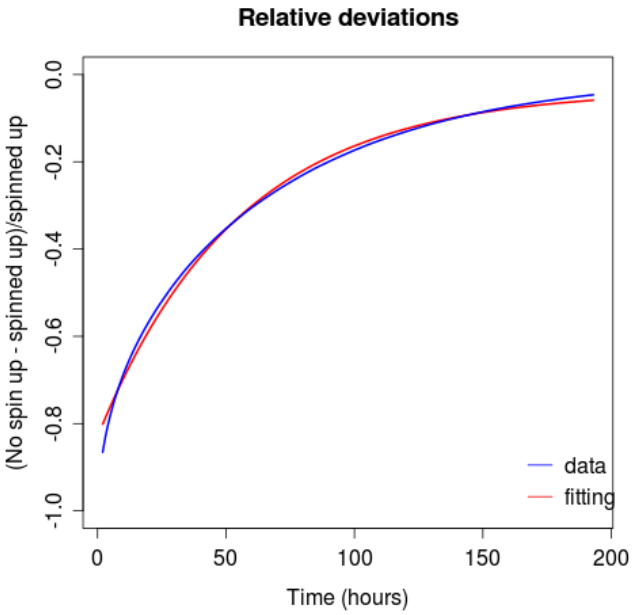

a) Relative deviation between w/o and w auto spin up initialization method and the exponential fitting for one domain cell

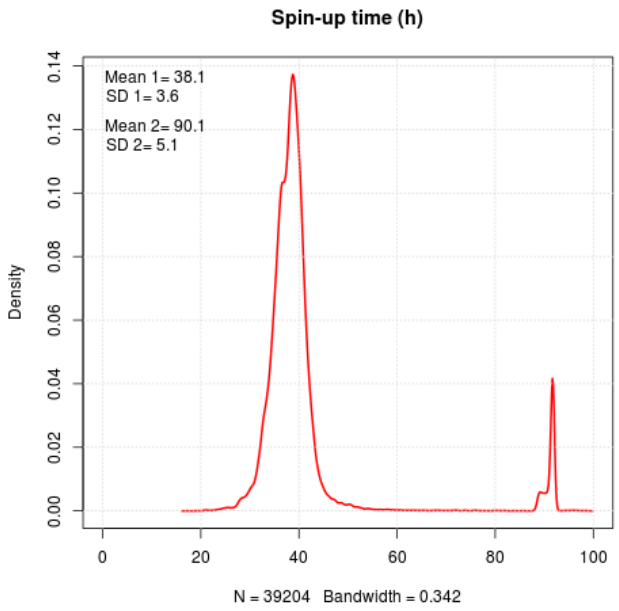

b) Probability distribution of the initialization half life for the whole domain.

Figure 3. Spin up time calculations; approach 1.

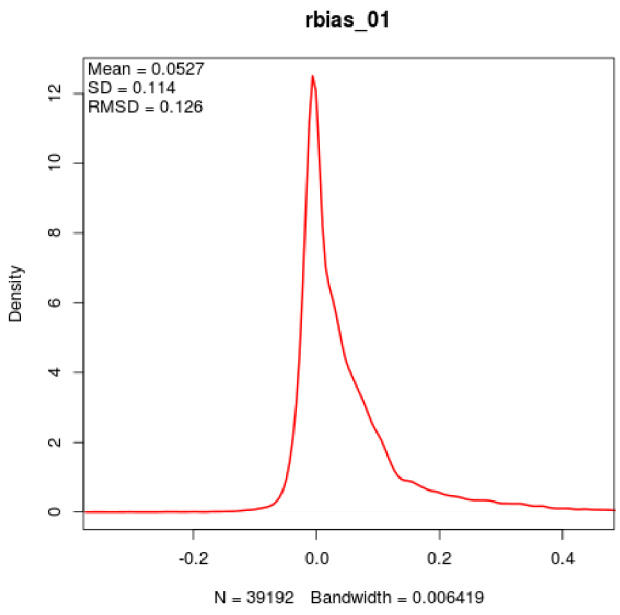

a) Probability distribution of relative differences between the fluxes calculated using 1 day and 8 days of meteorological data.

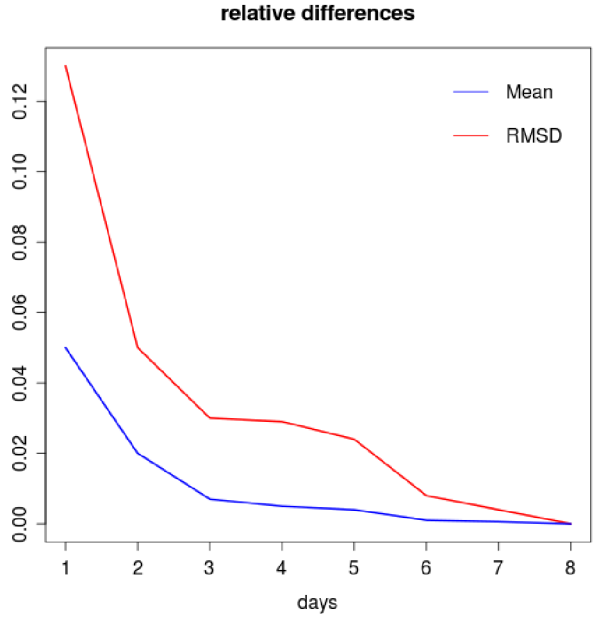

b) RBIAS and RMSD as a function of days used as spin-up time in the fluxes calculation

Figure 4. Spin up time calculations; approach 2.

3.2. Inventories comparison

The figure 5 shows the averaged fluxes differences for UHU-WRF, UHU-ERA and UnB inventories for the testing period (01/10/2009 - 10/10/2009). The upper part of the figure shows the spatial representation of calculated differences for each pair of inventories, and the lower part shows their probability distributions.

The UHU-ERA and UHU-WRF inventories comparison shows a BIAS of around -0.9 Bq m^{-2} h^{-1} with a RMSD around 18 Bq m^{-2} h^{-1}. Besides, the differences probability distribution is quite symmetric and zero centered. For its part, the UnB and UHU-WRF inventories comparison and the UnB and UHU-ERA inventories comparison show BIAS around 15 Bq m^{-2} h^{-1} and RMSD around 30 Bq m^{-2} h^{-1}. Both probability distributions are clearly shifted to positive values, indicating that the UnB inventory provides larger fluxes in comparison to the UHU-ERA and UHU-WRF inventories. In the last two cases, the largest differences are located in Spain. This fact could be derived from a UnB inventory radon fluxes overestimation in that country as published in Grossi et al., 2011.

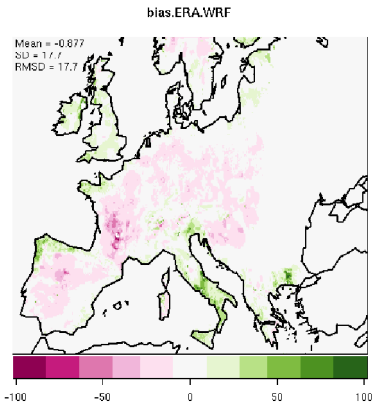

a) Fluxes differences between UHU-ERA and UHU-WRF inventories for the period

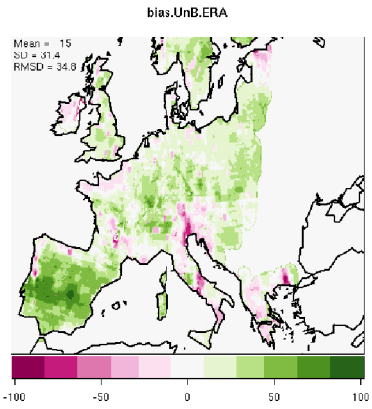

b) Fluxes differences between UnB and UHU-ERA inventories for the period

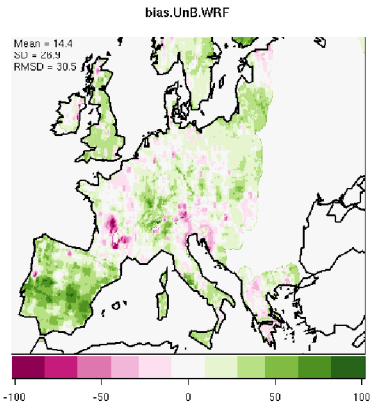

c) Fluxes differences between UnB and UHU-WRF inventories for the period

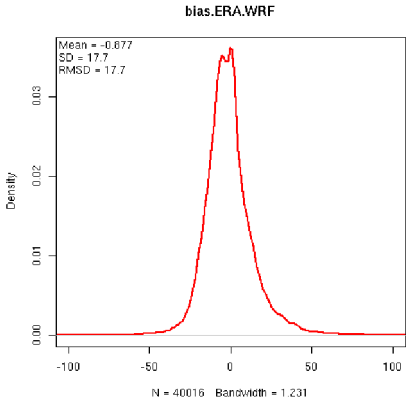

d) BIAS probability distribution

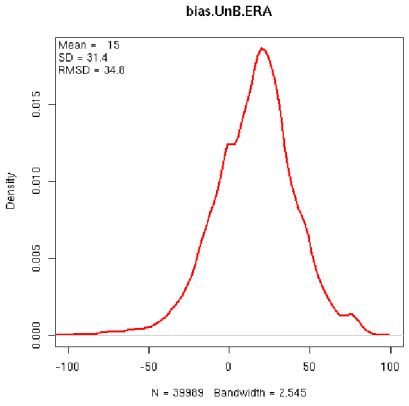

e) BIAS probability distribution

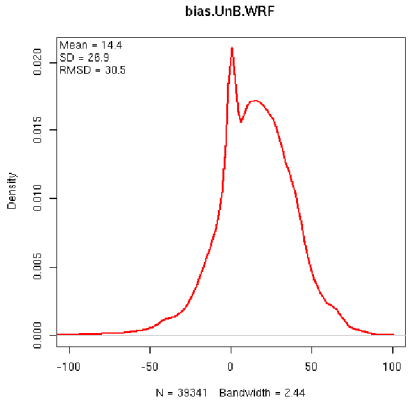

f) BIAS probability distribution

for fluxes predicted with UHU-ERA and UHU-WRF inventories for the period

for fluxes predicted with UnB and UHU-ERA inventories for the period

for fluxes predicted with UnB and UHU-WRF inventories for the period

Figure 5. Rn Fluxes differences between three inventories (UHU-WRF, UHU-ERA and UnB) in the period 01/09/2009 – 09/09/2009

3.2. Atmospheric radon concentration

As example, the figure 6 shows the simulated radon concentration in the low troposphere (model sigma level = 2) at 23:00 h UTC of 01/12/2008 using the UHU-WRF radon flux inventory. Enhanced simulated values can be seen over continents, as no radon is emitted over the oceans.

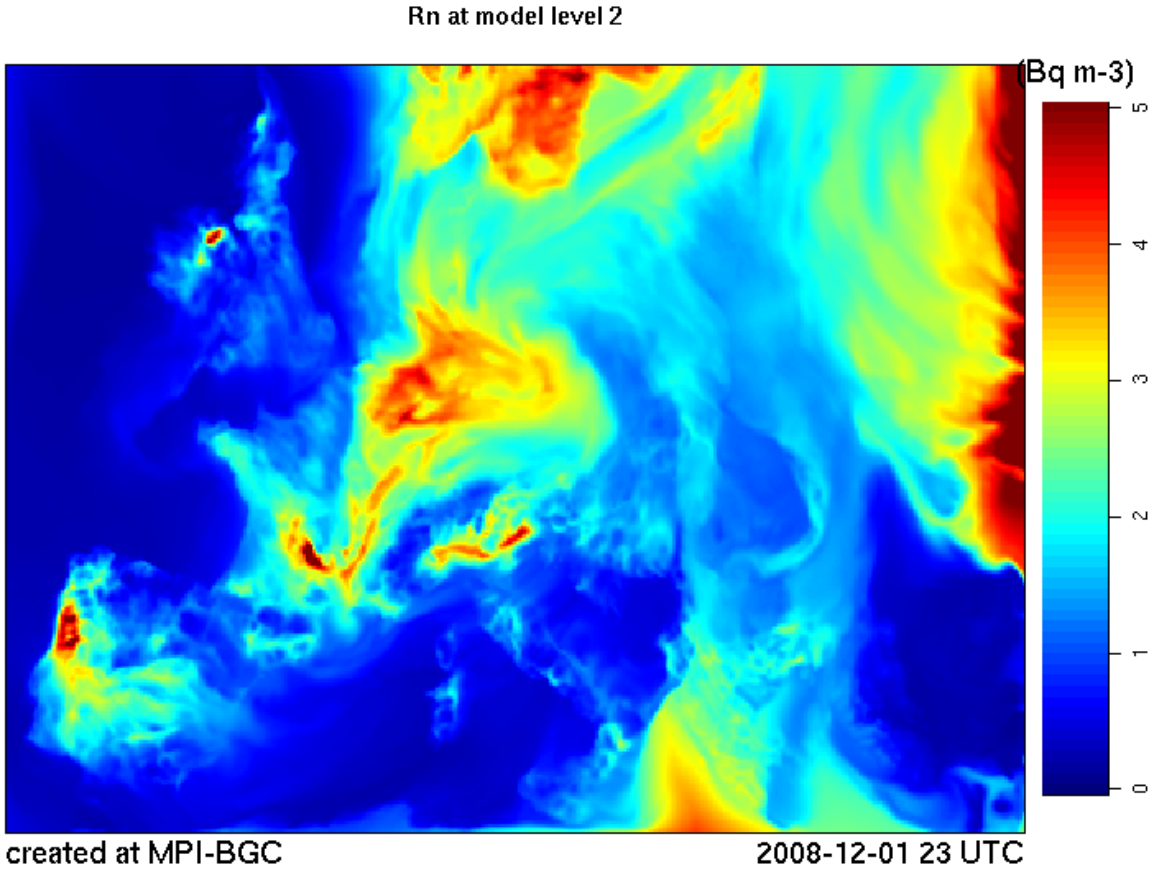

Figure 6. Simulated radon concentration (Bq m^{-3}) in the low troposphere (model sigma level = 2) at 23:00 h UTC of 01/12/2008 using the UHU-WRF radon flux inventory.

3.2.1. Overall behavior

In general, the four radon flux inventories tested show similar performances, table 2. The more probable value of the differences (MODE) has the lowest value of -0.004 Bq m^{-3} for the UHU-WRF inventory and the highest value for the UnB inventory, 0.14 Bq m^{-3}. Besides, the standard deviation is close to 1 Bq m^{-3} for all the inventories, being the highest value of 1.04 Bq m^{-3} for UnB and UHU-ERA inventories and lowest value of 0.99 Bq m^{-3} for UHU-WRF. The RMSD has the lowest value of 1.01 Bq m^{-3} for the UHU-WRF and CTE inventory and the highest value of 1.06 Bq m^{-3} for the UHU-ERA inventory.

The overall RMSD is slightly higher than 1 Bq m^{-3}. Besides, the BIAS shows us the differences are negative for the UHU-WRF, UHU-ERA and CTE inventories and positives for UnB. Nevertheless, the most probable value (MODE) reveals that the probability distributions of differences are slightly asymmetric since they are different of the BIAS. Thus, the mode for UHU-WRF is almost zero, while for the another inventories it is slightly positive.

With this, we can assume the probability distribution of differences are slightly deviated towards positive values for the UnB inventory and towards negative ones for the another inventories.

Table 2. Inventories score evaluation

Inventories	**BIAS (Bq m^{-3})**	**SD (Bq m^{-3})**	**RMSD (Bq m^{-3})**	**MODE (Bq m^{-3})**	**P5 (Bq m^{-3})**	**P95 (Bq m^{-3})**
UHU-WRF	-0.26	0.99	1.01	-0.004	-2.19	0.87
UHU-ERA	-0.23	1.04	1.06	0.064	-2.28	0.96
UnB	0.10	1.04	1.04	0.144	-1.80	1.52
CTE	-0.16	1.00	1.01	0.039	-2.10	0.99

The figure 7.a shows the probability distribution of the differences for each inventory. As it said before, the asymmetry is quite small in all of them. The UHU-WRF, UHU-ERA and CTE inventories show quite similar distributions, being the UHU-WRF the narrowest one, as it shown by the standard deviation (0.99 Bq m^{-3}) The UnB inventory shows the most different distribution. Thus, the asymmetry is due to more probable positive values and, thus, the cumulated probability distribution shows more than 60% of values are higher than zero, (figure 7.b). Besides, the 5-percentile is around -2 Bq m^{-3} for all inventories while the 95-percentile is less than 1 Bq m^{-3} for the UHU-WRF, UHU-ERA and CTE inventories and it is around 1.5 Bq m^{-3} for the UnB inventory.

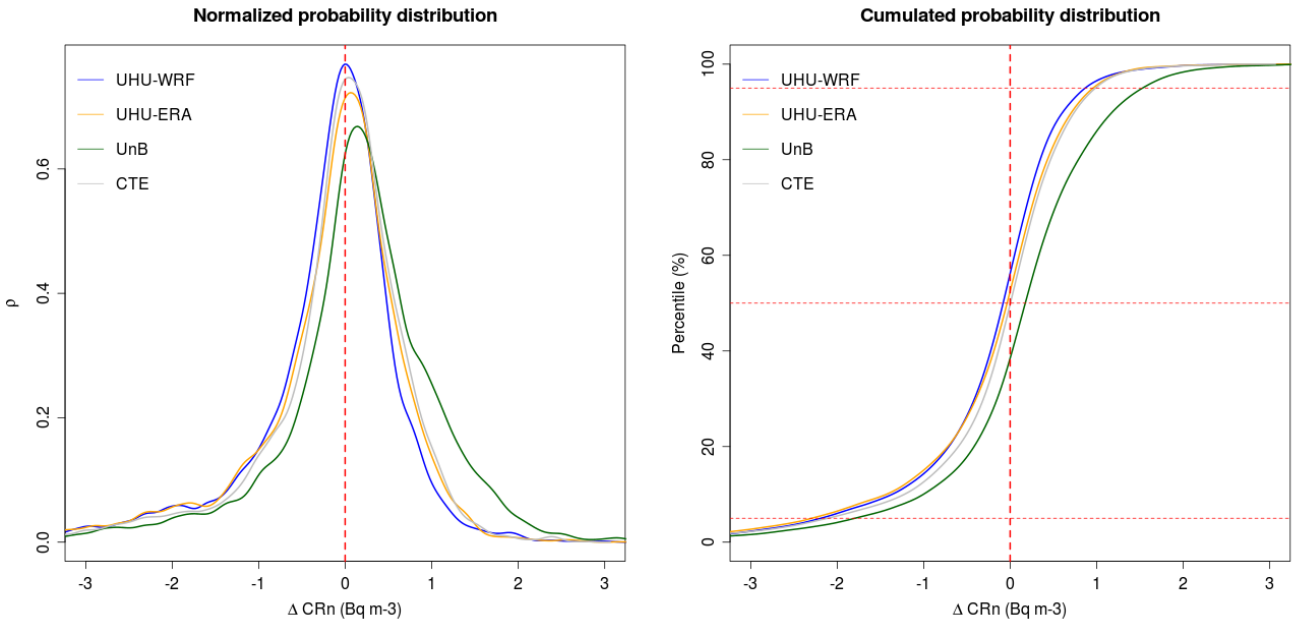

a) Normalized probability distribution of differences

b) Cumulated probability distribution of differences

Figure 7. Normalized and cumulated probability distributions of deviations between simulated and measured radon concentration corresponding with all station and periods for each inventory

3.2.2 Performances by simulated period

The performances by simulated period are quite similar to the overall behavior showed before. Nevertheless, we can see difference between them. Thus, the lowest values of the inventories RMSD are in May, while highest ones are in October. The biggest difference between inventories RMSD are in February, with 0.94 Bq m^{-3} for UHU-WRF and 1.1 Bq m^{-3} for UnB, and in October with 1.2 Bq m^{-3} for UnB and 1.36 Bq m^{-3} for UHU-ERA.

The inventories RMSD show an interesting characteristic of the simulation system: the RMSD differences between periods are in the same order of magnitude as the RMSD differences between inventories. This result tells us that the specific meteorological conditions are influencing the overall behavior of the simulation system.

Concretely, in the 2009/10/10 period it is possible to see an underestimation of the radon concentrations, simulated employing zero boundary conditions, around 5% respect to the value obtained employing TM3 boundary conditions. This fact has a double implication: a) Providing boundary conditions have a positive effect on simulated radon concentration and, b) providing wrong boundary conditions can affect negatively the simulated results.

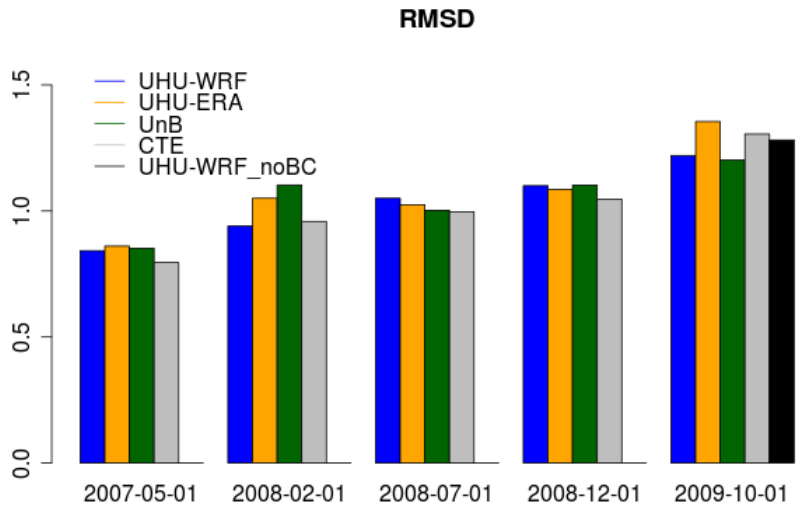

Figure 8. RMSD for each inventory and simulated period (Bq m^{-3})

3.2.3. Analysis of causes for mismatch

In this part, we investigate in detail the radon time series evolution in order to obtain a deeper knowledge about the simulation system performances and the possible reasons for the observed mismatch between simulated and observed radon concentrations during specific events.

a) Strong accumulations

In general, the strong accumulation processes are badly reproduced by the model. For instance, the figure 9 shows the radon concentration is underestimated in the nights. This fact is common to all inventories, thus it is possible to assume that the observed nocturnal accumulation processes are stronger than simulated due to that the nocturnal stable layer is not properly reproduced and the planetary boundary layer (PBL) height is overestimated by the model. Besides, such a situation can be extended over several day as can be seen in the figure 9.b (days 2 and 3)

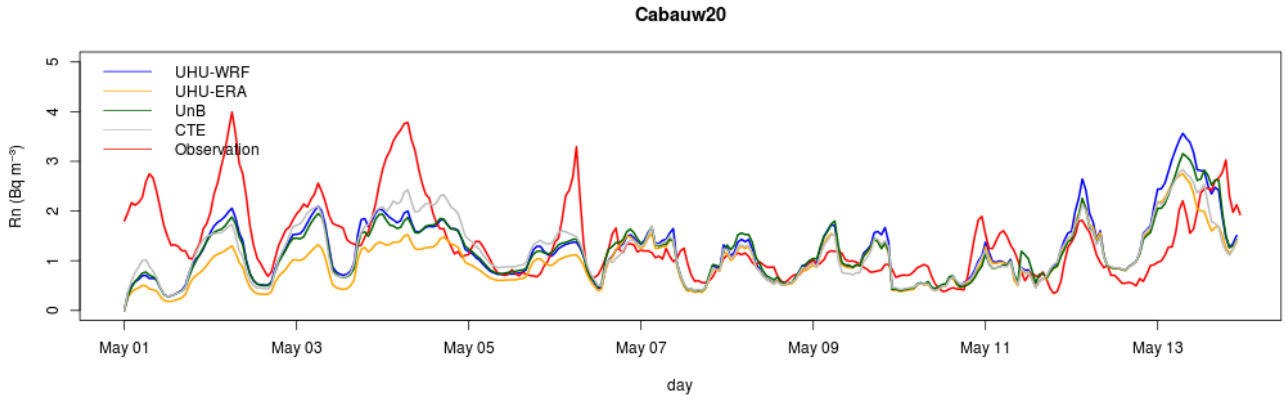

a) Simulated and observed Radon concentration evolution for Cabauw (20 m) during the period 01/05/2007-14/05/2007

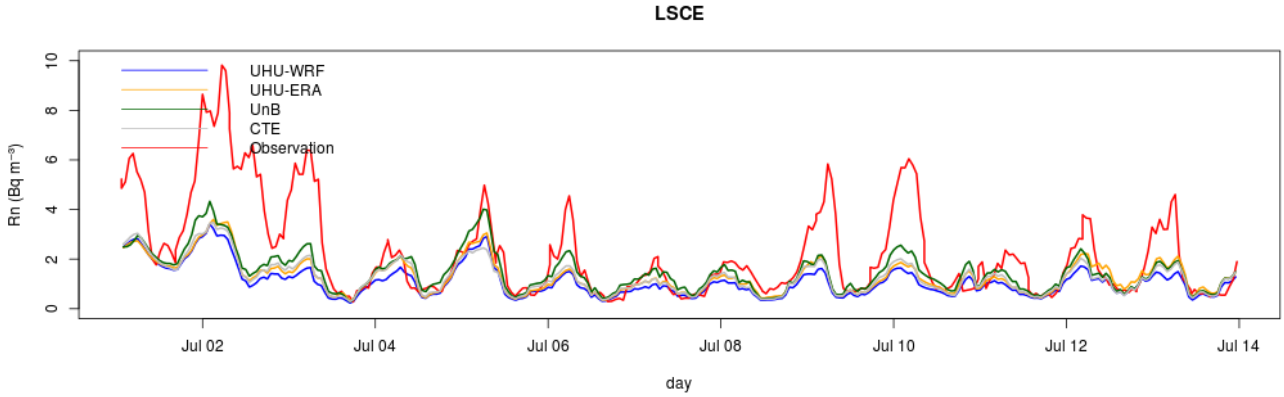

b) Simulated and observed Radon concentration evolution for Gif (LSCE) during the period 01/07/2008-14/07/2008

Figure 9. Badly reproduced strong accumulation examples

b) Source term overestimation

In contrast to the previously described situation, the figure 10 shows large differences between the radon concentration obtained by simulation employing different radon flux inventories. We found this kind of behavior typically in the wet months for the European domain. This results from the radon flux dependence on the soil water content (López-Coto, 2011) The UnB inventory and to a lesser extent the UHU-ERA and the CTE inventories are overestimating the source term. All of them provide in general higher values than measured. Meanwhile, the UHU-WRF inventory is taking into account the actual soil humidity simulated by WRF and in fact provides values of radon concentration closer to the observations in comparison to the other inventories.

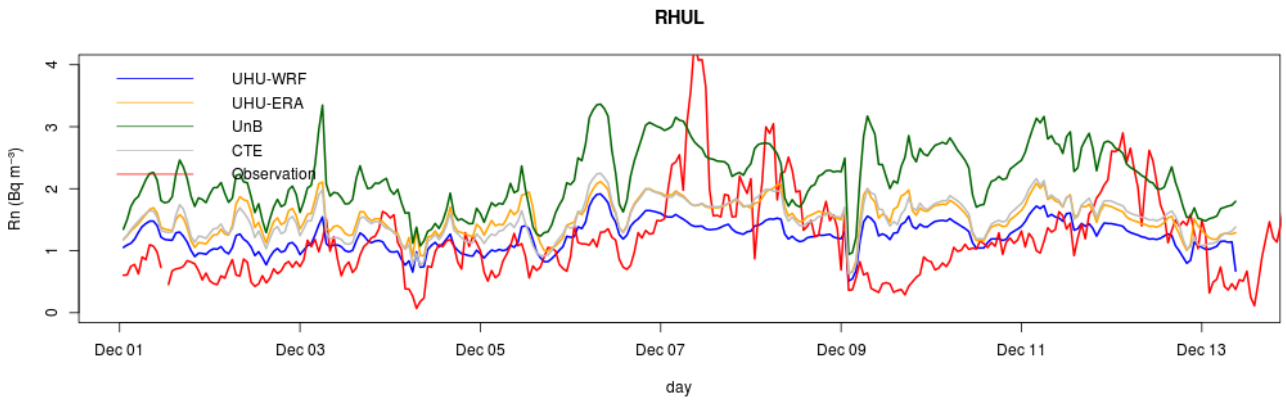

a) Simulated and observed Radon concentration evolution for RHUL during the period 01/12/2008-14/12/2008

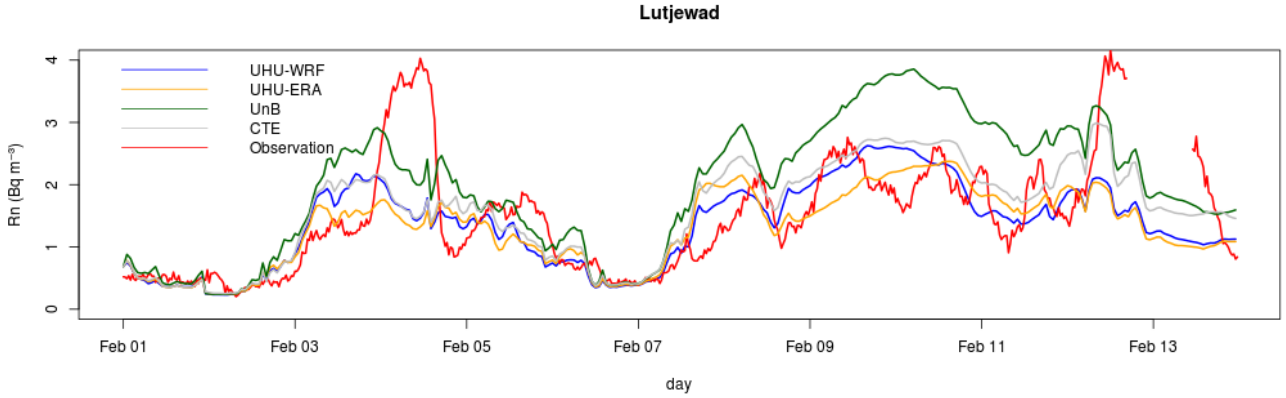

b) Simulated and observed Radon concentration evolution for Lutjewad during the period 01/02/2008-14/02/2008

Figure 10. Source term overestimation examples

c) Badly reproduced horizontal transport

Sometimes, the atmospheric model can not reproduce properly the horizontal transport. This could be due to several reasons; for instance, non-resolved local convective transport, wind magnitude errors, wrong boundary conditions or near region radon source term errors. We should assume that this fact could appear both as ventilation and as enrichment events, nevertheless the enrichment events are harder to identify it than the ventilation events. The figure 11 shows three ventilation events not reproduced by the model (days 8, 10 and 13). These events could be due to sea air masses horizontal advection induced by the synoptic structure or an enhanced vertical convective transport induced by the passing of a low pressure cell.

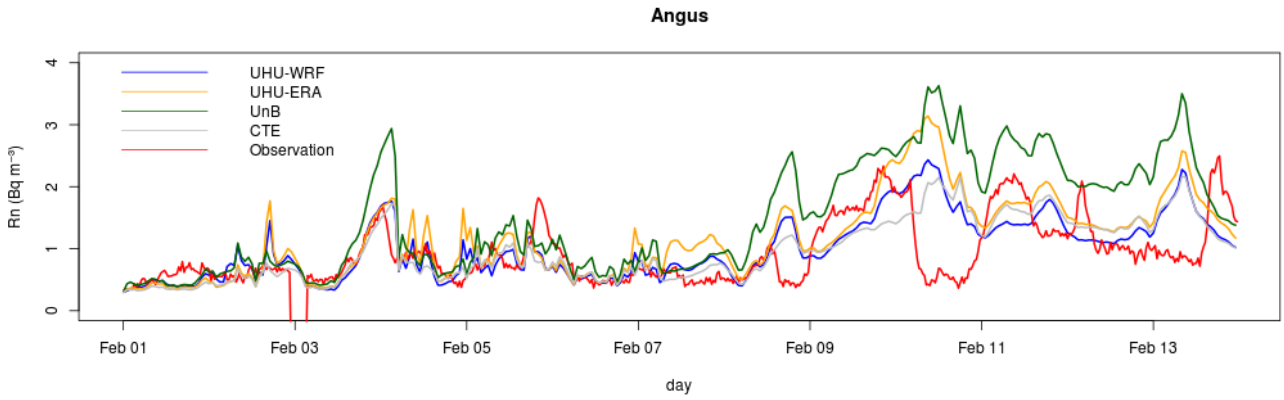

Figure 11. Simulated and observed Radon concentration evolution for Angus during the period 01/02/2008-14/02/2008. Badly reproduced horizontal transport example.

d) Initial and boundary conditions effects

The figure 12.a shows the effect of using a zero initial condition in the simulated radon concentration. The first day evolution is underestimated for all inventories. In this case, at least 24 hours are required to get realistic conditions in the simulation. Besides, the boundary conditions employed are affecting the general performance of the model. The figure 12.b shows a general underestimation of the radon concentrations simulated employing zero boundary conditions, in contrast to those obtained using TM3 boundary conditions.

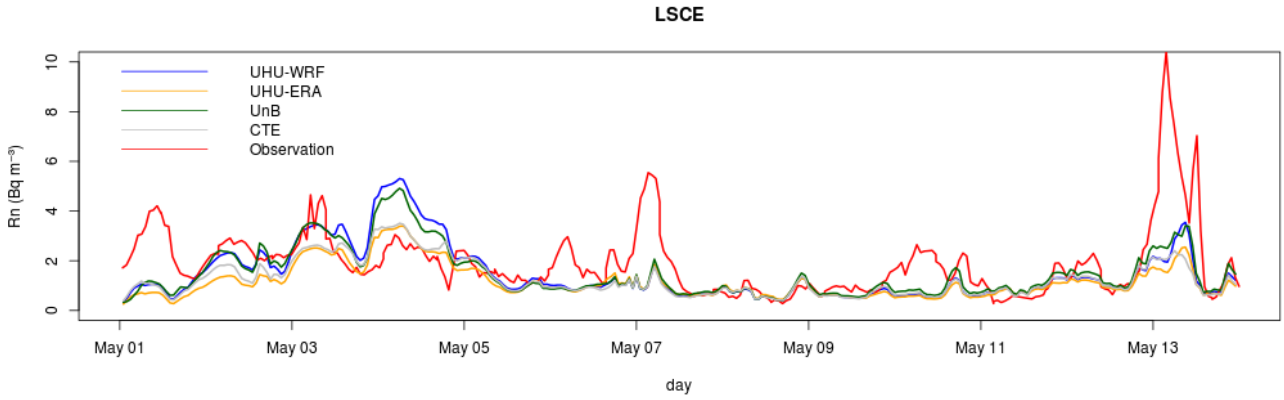

a) Simulated and observed Radon concentration evolution for Gif (LSCE) during the period 01/05/2007-14/05/2007

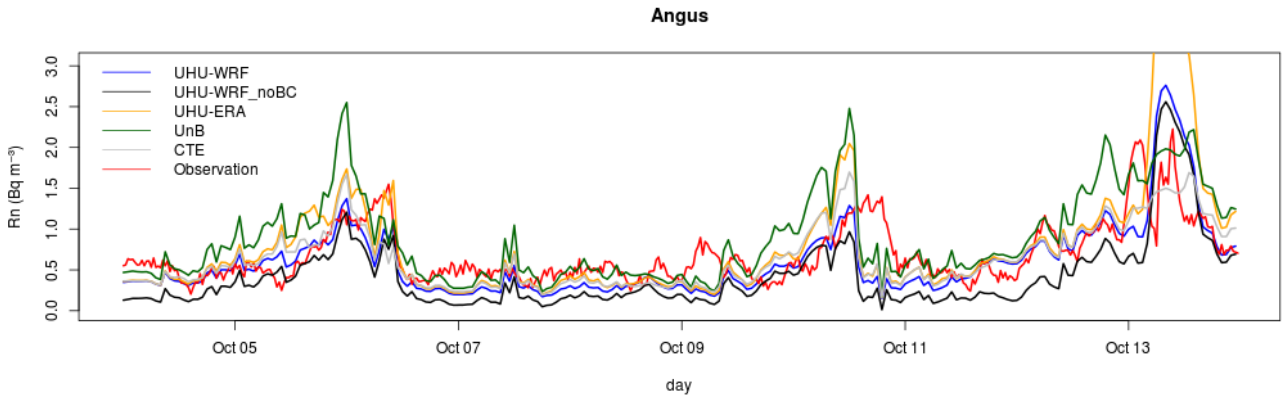

b) Simulated and observed Radon concentration evolution for Angus during the period 04/10/2009-14/10/2009

Figure 12. Initial and boundary condition effects examples. Both simulation periods were initialized with zero initial condition but only the UHU-WRF_noBC test case was initialized with zero boundary conditions.

4. Conclusions

In this work, a time dependent radon flux inventory has been evaluated, showing in general a good agreement with previous inventories. Besides, the radon decay process has been included into WRF-GHG model and the time dependent inventory and other 3 static inventories have been coupled to WRF-CHEM-GHG in offline mode using TM3 derived initial and boundary conditions.

The auto spin up initialization method employed in the time dependent radon flux calculation code has been shown to reduce the initialization time from around eleven days to only one hour; nevertheless, the test case shows that the auto initialized radon model needs at least one running day for stabilizing the solution.

In order to validate the simulation system results and evaluate the inventories performances, five 13-days periods have been simulated and the results have been compared against radon concentration measurements from 6 stations.

The overall RMSD is slightly higher than 1 Bq m^{-3}. Besides, the BIAS is negative for the UHU-WRF, UHU-ERA and CTE inventories and positives for UnB. Nevertheless, the most probable value (MODE) reveal that the probability distributions of differences are slightly asymmetric since they are different from the BIAS. Thus, the mode for UHU-WRF is almost zero, while for the other European inventories it is slightly positive.

The RMSD differences between periods are in the same order of magnitude as the RMSD differences between inventories. This result tells us that the specific meteorological conditions are influencing the overall behavior of the simulation system.

Different events of the simulated time-series, during which the simulations indicated especially large deviations from the observations, have been analyzed in detail in order to assess potential reasons for mismatches. In general, the strong accumulation processes are badly reproduced by the model, generally during nights. This fact is probably due to the fact that the stable layer is not properly reproduced and the planetary boundary layer (PBL) height is overestimated by the model.

Large differences could be found between the radon concentrations obtained by employing different radon flux inventories during the typical European wet months. This fact is due to the dependence of radon flux on the soil water content. Only the time-dependent implementation of UHU-WRF allows for capturing this important influence of meteorology on radon exhalation rates.

Sometimes, the atmospheric model can not properly reproduce horizontal transport. This could be due to several reasons; for instance, non-resolved local convective transport, wind magnitude errors, wrong boundary conditions or near region radon source term errors.

Furthermore, the boundary conditions employed are affecting the general performance of the model.

Including the radon decay process into WRF-CHEM along with the time dependent radon flux inventory and testing the simulations results against radon data time series from experimental measurement stations have been a fundamental first step towards an operational evaluation of model performance with high relevance for estimation of GHG exchange fluxes derived from atmospheric observations.

Ultimately, the results obtained in this project could serve as starting point for several research lines related to TTORCH network subjects such as transport model validations and GHG source estimation, as well as other research lines not directly related to TTORCH but with high interest in the scientific community as radioactive aerosol transport, radioactive waste management or air ionization simulations and its relation with the aerosol nucleation.

5. References

Ahmadov, R., Gerbig, C., Kretschmer, R., Koerner, S., Neininger, B., Dolmann, A.J. and Sarat, C., (2007). Mesoscale covariance of transport and CO2 fluxes: Evidence from observations and simulations using the WRF-VPRM coupled atmosphere-biosphere model. J. Geophys. Res., 112, D22107, doi:10.1029/2007JD008552.

Beck, V., Koch, T., Kretschmer, R., Marshall, J., Ahmadov, R., Gerbig, C., Pillai, D. and Heimann, M. (2011) The WRF Greenhouse Gas Model (WRF-GHG). Technical Report No. 25, Max Planck Institute for Biogeochemistry, Jena, Germany, downloaded from http://www.bgc-jena.mpg.de/bgc-systems/pmwiki2/uploads/Publications/25.pdf

Bousquet, P., Ciais, P., Miller, J.B., Dlugokencky, E.J., Hauglustaine, D.A., Prigent, C., van der Werf, G., Peylin, P., Brunke, E., Carouge, C., Langenfelds, R.L., Lathiere, J., Papa, F., Ramonet, M., Schmidt, M., Steele, L.P., Tyler, S.C., White, J.W.C. (2006) Contribution of anthropogenic and natural sources methane emissions variability. Nature 443, 439–443.

Conen, F., Robertson, L.B., (2002). Latitudinal distribution of radon-222 flux from continents. Tellus 54 (B), 127–133.

Dentener, F., Feichter, J., Jeuken, A., (1999) Simulation of the transport of Rn-222 using on-line and off-line global models at different horizontal resolutions: a detailed comparison with measurements. Tellus 51 (B), 573–602.

Grell, G. A. and Devenyi, D. (2002) A generalized approach to parameterizing convection combining ensemble and data assimilation techniques Geophys. Res. Lett., 29, 14, 1693, 10.1029/2002GL015311.

Grossi, C., Vargas, A., Camacho, A., López-Coto, I., Bolivar, J.P., Xia, I., Conen, F. (2011) Intercomparison of different direct and indirect methods to determines 222Rn flux from soils. Radiation Measurements, 46, 112 – 118

Gurney, K.R., Law, R.M., Denning, A.S., Rayner, P.J., Baker, D., Bousquet, P., Bruhwiler, L., Chen, Y.H., Ciais, P., Fan, S., Fung, I.Y., Gloor, M., Heimann, M., Higuchi, K., John, J., Maki, T., Maksyutov, S., Masarie, K., Peylin, P., Prather, M., Pak, B.C., Randerson, J., Sarmiento, J., Taguchi, S., Takahashi, T., Yuen, C.W. (2002) Towards robust regional estimates of CO2 sources and sinks using atmospheric transport models. Nature 415, 626–630.

Heimann, M. and Körner, S. (2003). The Global Atmospheric Transport Model TM3: Model Description and User Manual. Max Planck Inst. for Biogeochem. (MPI-BGC), Jena, Germany

Jacob, D.J., Prather, M.J., Rasch, P.J., Shia, R.L., Balkanski, Y.J., Beagley, S.R., Bergmann, D.J., Blackshear, W.T., Brown, M., Chiba, M., Chipperfield, M.P., deGrandpre, J., Dignon, J.E., Feichter, J., Genthon, C., Grose, W.L., Kasibhatla, P.S., Kohler, I., Kritz, M.A., Law, K., Penner, J.E., Ramonet, M., Reeves, C.E., Rotman, D.A., Stockwell, D.Z., VanVelthoven, P.F.J., Verver, G., Wild, O., Yang, H., Zimmermann, P. (1997). Evaluation and intercomparison of global atmospheric transport models using Rn-222 and other short-lived tracers. Journal of Geophysical Research 102, 5953–5970

Kessler, E., 1969: On distribution and continuity of water substance in atmospheric circulations. American Meteorological Society, Mereorol. Monogr., 10; 32, 84.

Levin, I., Born, M., Cuntz, M., Langendörfer, U., Mantsch, S., Naegler, T., Schmidt, M., Varlagin, A., Verclas, S., and Wagenbach, D. (2002) Observations of atmospheric variability and soil exhalation rate of radon-222 at a Russian forest site, Tellus B, 54, 462–475, 2002.

López-Coto, I. (2011) Spatial and temporal variability of radon sources and concentrations in the low atmosphere. Ph D Thesis. University of Huelva. ISBN: 978-84-15147-74-9

Nakanishi, M. and Niino, H., (2006) “An Improved Mellor–Yamada Level-3 Model: Its Numerical Stability and Application to a Regional Prediction of Advection Fog", Boundary-Layer Meteorology, 119, 397-407.

Rasch, P., Feichter, J., Law, K., Mahowald, N., Penner, J., Benkovitz, C., Genthon, C., Giannakopoulos, C., Kasibhatla, P., Koch, D., Levy, H., Maki, T., Prather, M., Roberts, D.L., Roelofs, G.-J., Stevenson, D., Stockwell, Z., Taguchi, S., Kritz, M., Chipperfield, M., Baldocchi, D., McMurry, P., Barrie, L., Balkanski,

Y., Chatfield, R., Kjellstrom, E., Lawrence, M., Lee, H.N., Lelieveld, J., Noone, K.J., Seinfeld, J., Stenchikov, G., Schwartz, S., Walcek, C., Williamson, D., (2000) A comparison of scavenging and deposition processes in global models: results from the WCRP Cambridge Workshop of 1995. Tellus 52 (B), 1025–1056.

Rodenbeck, C., Houweling, S., Gloor, M., Heimann, M. (2003) CO2 flux history 1982 – 2001 inferred from atmospheric data using a global inversion of atmospheric transport. Atmospheric Chemistry and Physics 3, 1919–1964.

Schmidt, M., Glatzel-Mattheier, H., Sartorius, H., Worthy, D. E. & Levin, I. (2001) Western European N2O emissions—a top down approach based on atmospheric observations. J. Geophys. Res. 106, 5507–5516.

Skamarock, W. C., Klemp, J. B., Dudhia, J., Gill, D. O., Barker, D. M., Duda, M. G., Huang, X-Y., Wang, W., and Powers, J. G. (2008) A Description of the Advanced Research WRF Version 3, NCAR Technical Note, NCAR/TN–475+STR.

Szegvary, T., Conen, F., Ciais, P. (2009) European 222Rn inventory for applied atmospheric studies. Atmospheric Environment; 43; 1536–1539

Whittlestone, S. and Zahorowski, W. (1998). Baseline radon detectors for shipboard use: Development and deployment in the First Aerosol Characterization Experiment (ACE 1). Journal of Geophysical Research, 103(D13), 16,743-16,751.

Annex

In this annex, the simulated and observed radon concentration time series obtained for each station and simulated period are showed.

A.1. Episode 01/10/2009 - 14/10/2009

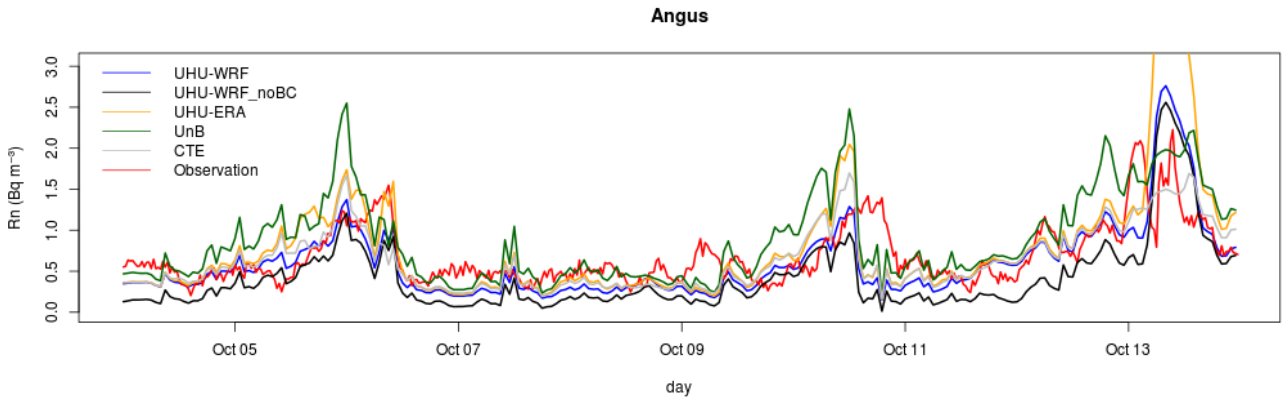

Figure A.1.a) Simulated and observed Radon concentration evolution for Angus during the period 04/10/2009-14/10/2009

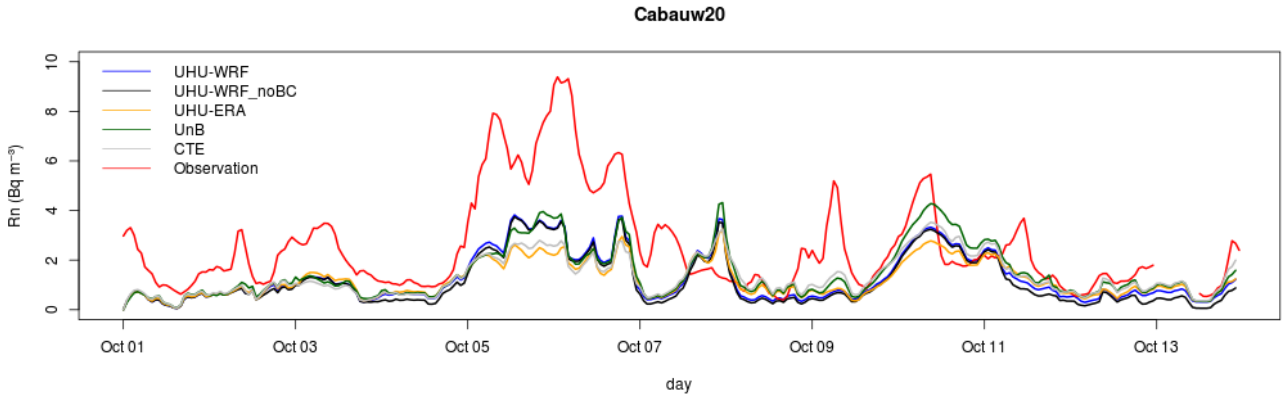

Figure A.1.b) Simulated and observed Radon concentration evolution for Cabauw (20 m) during the period 01/10/2009-14/10/2009

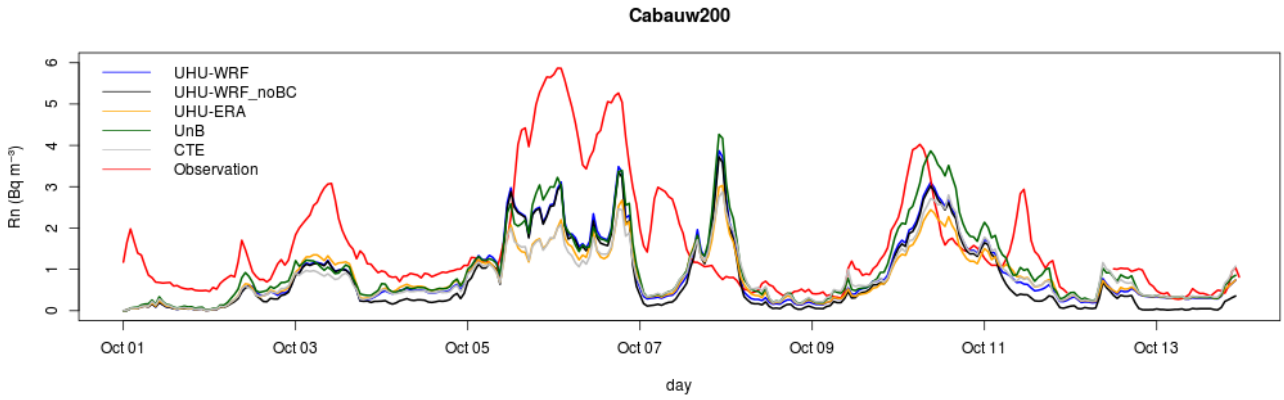

Figure A.1.c) Simulated and observed Radon concentration evolution for Cabauw (200 m) during the period 01/10/2009-14/10/2009

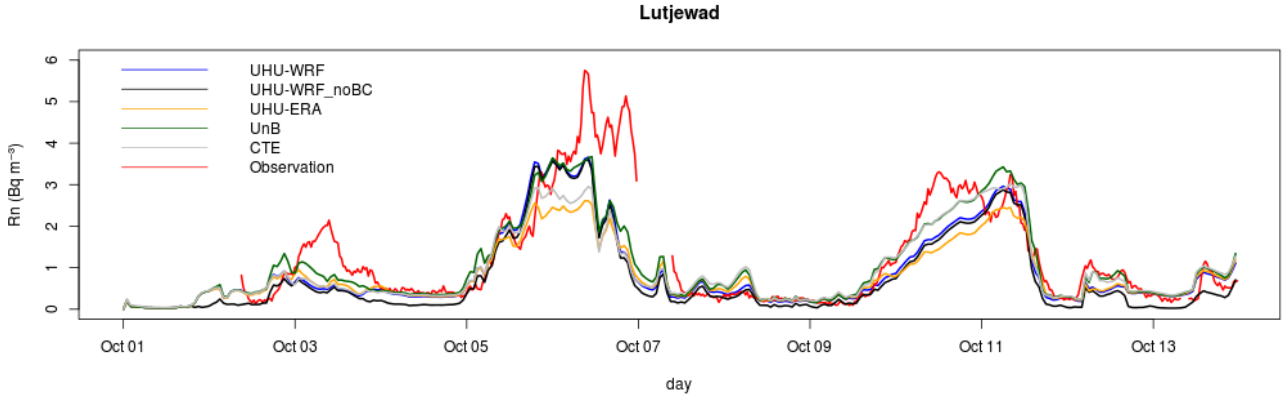

Figure A.1.d) Simulated and observed Radon concentration evolution for Lutjewad during the period 01/10/2009-14/10/2009

A.2. Episode 01/12/2008 - 14/12/2008

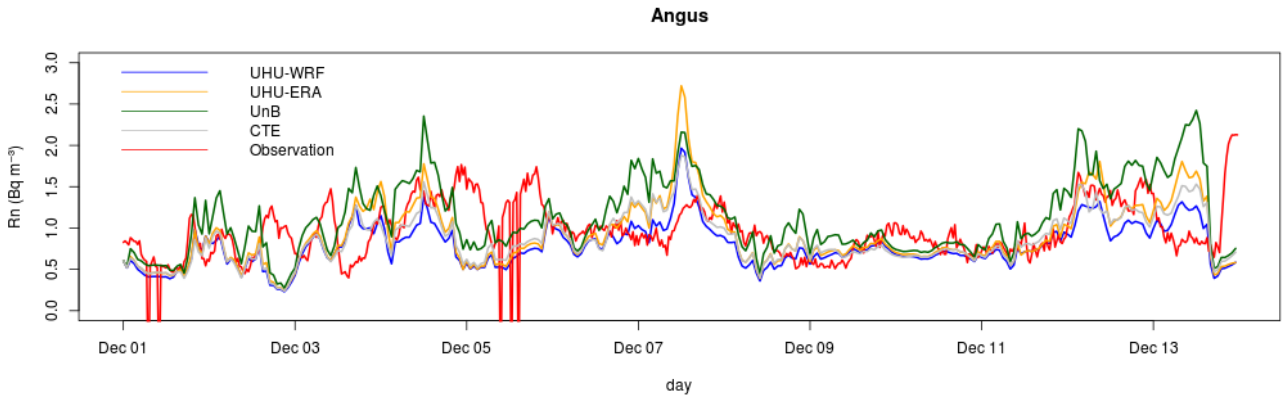

Figure A.2.a) Simulated and observed Radon concentration evolution for Angus during the period 01/12/2008-14/12/2008

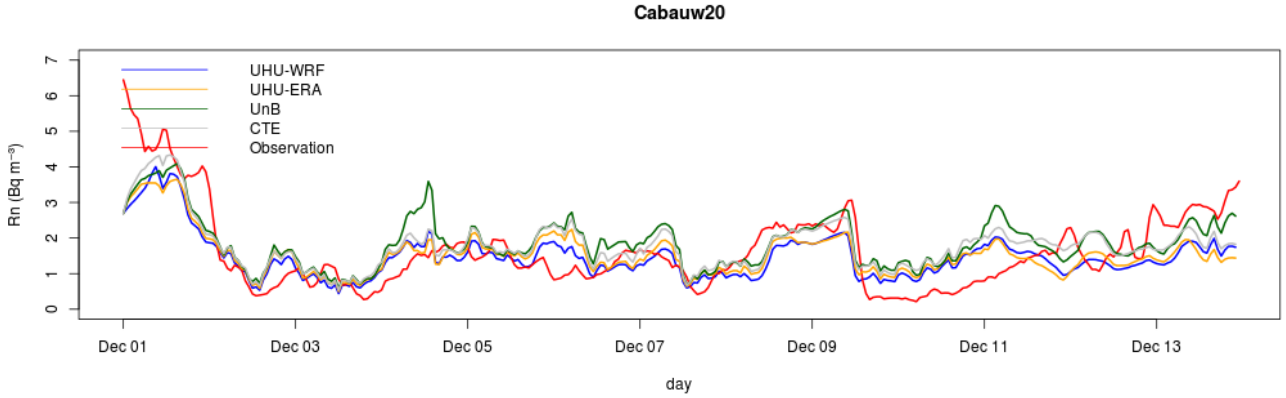

Figure A.2.b) Simulated and observed Radon concentration evolution for Cabauw (20 m) during the period 01/12/2008-14/12/2008

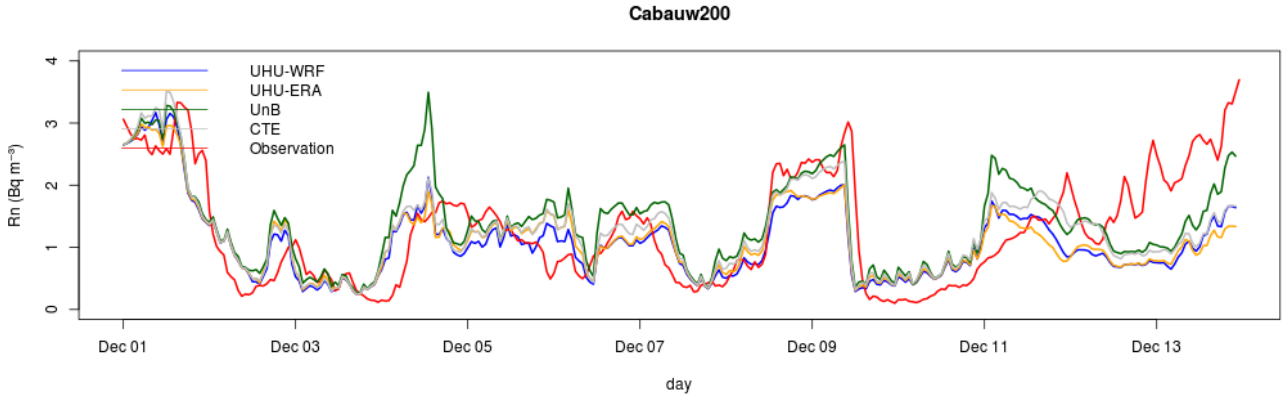

Figure A.2.c) Simulated and observed Radon concentration evolution for Cabauw (200 m) during the period 01/12/2008-14/12/2008

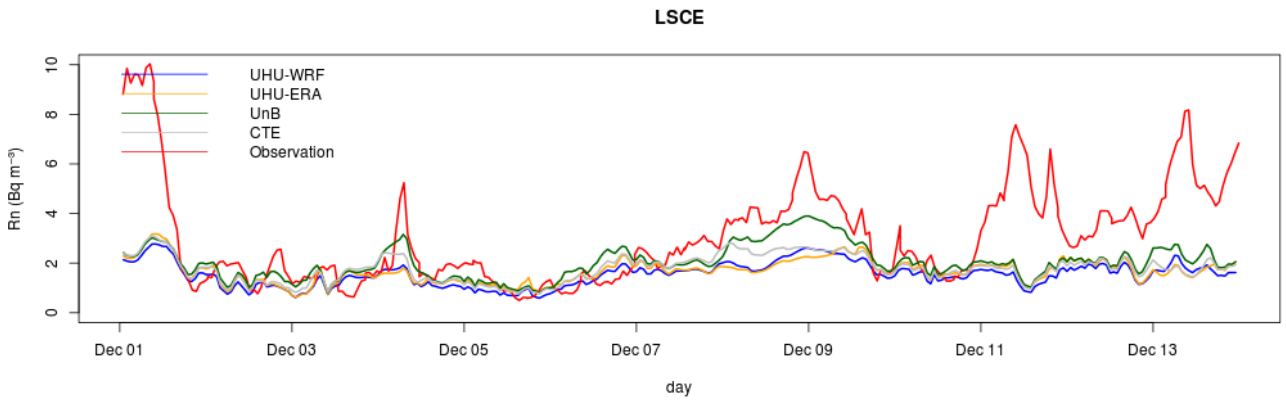

Figure A.2.d) Simulated and observed Radon concentration evolution for LSCE during the period 01/12/2008-14/12/2008

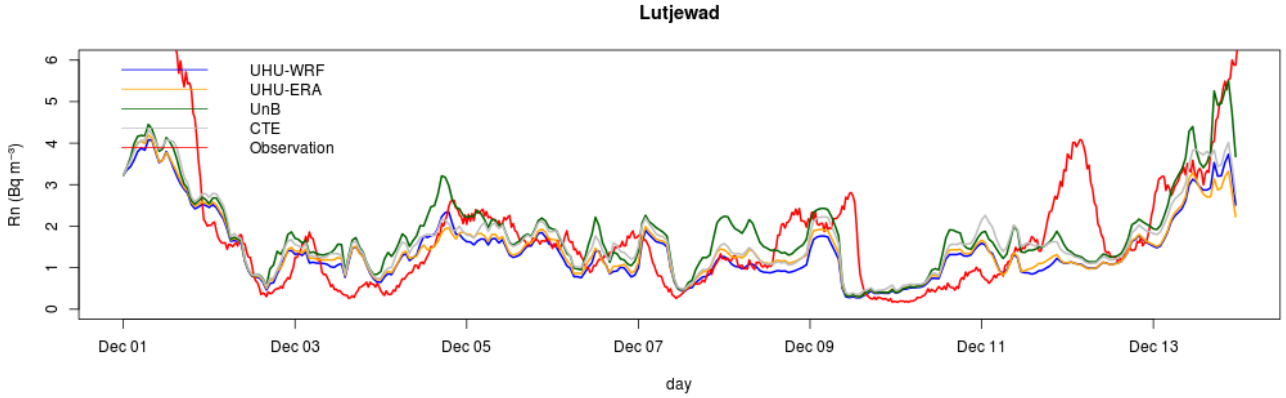

Figure A.2.e) Simulated and observed Radon concentration evolution for Lutjewad during the period 01/12/2008-14/12/2008

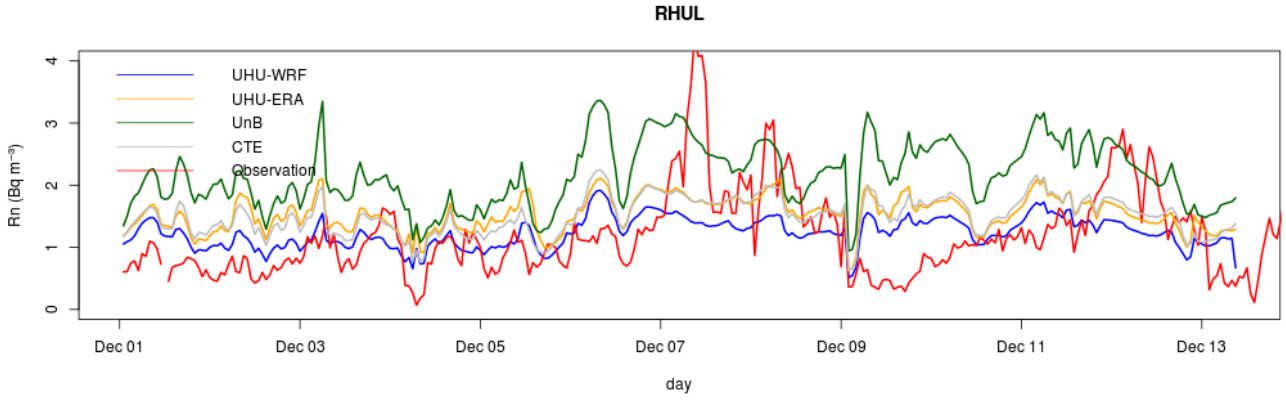

Figure A.2.f) Simulated and observed Radon concentration evolution for RHUL during the period 01/12/2008-14/12/2008

A.3. Episode 01/07/2008 - 14/07/2008

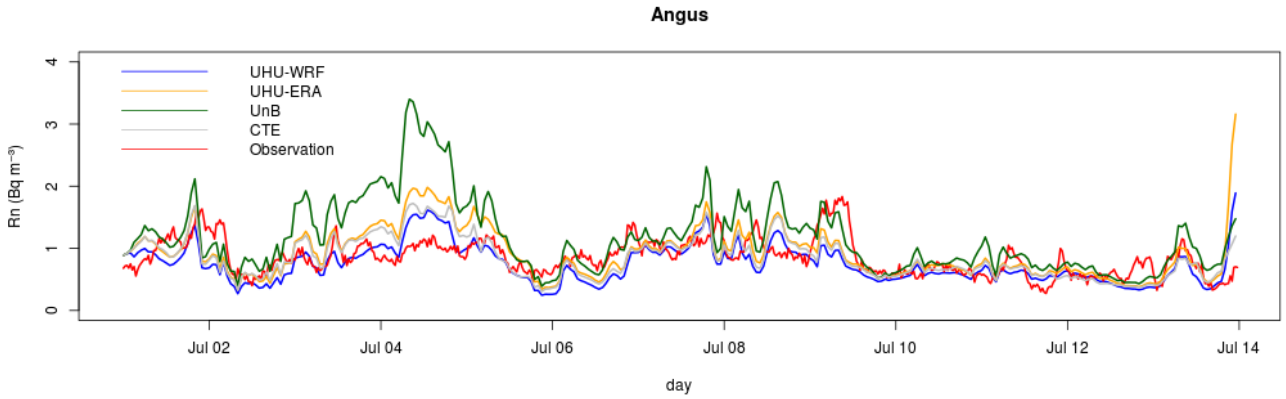

Figure A.3.a) Simulated and observed Radon concentration evolution for Angus during the period 01/07/2008-14/07/2008

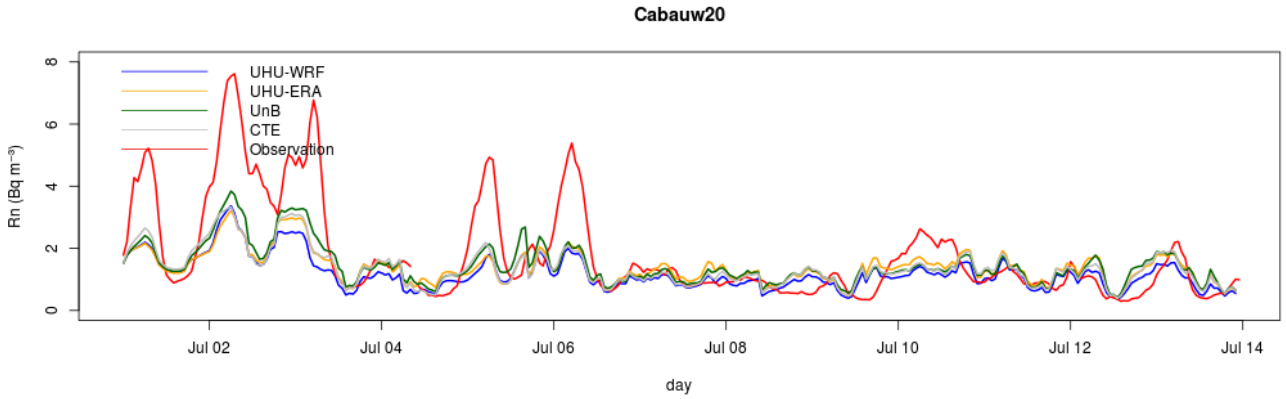

Figure A.3.b) Simulated and observed Radon concentration evolution for Cabauw (20 m) during the period 01/07/2008-14/07/2008

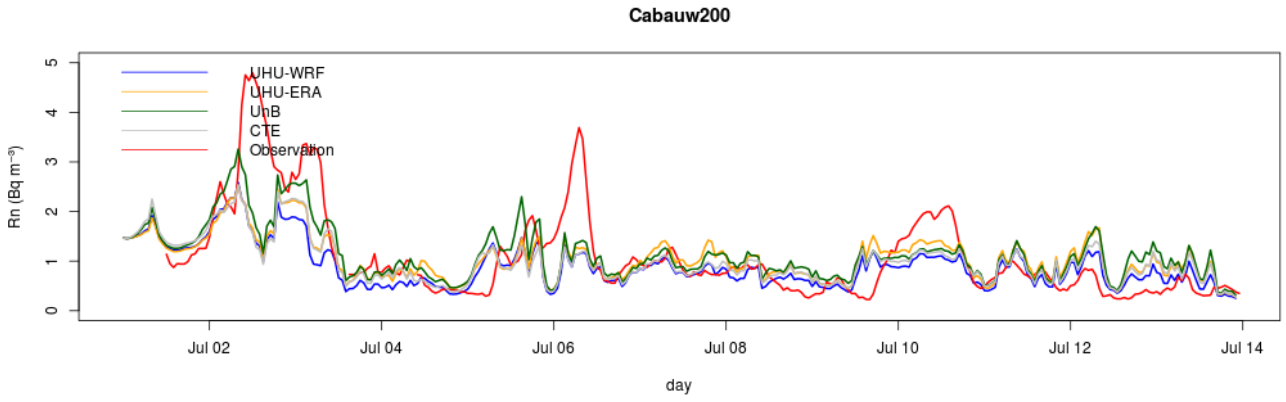

Figure A.3.c) Simulated and observed Radon concentration evolution for Cabauw (200 m) during the period 01/07/2008-14/07/2008

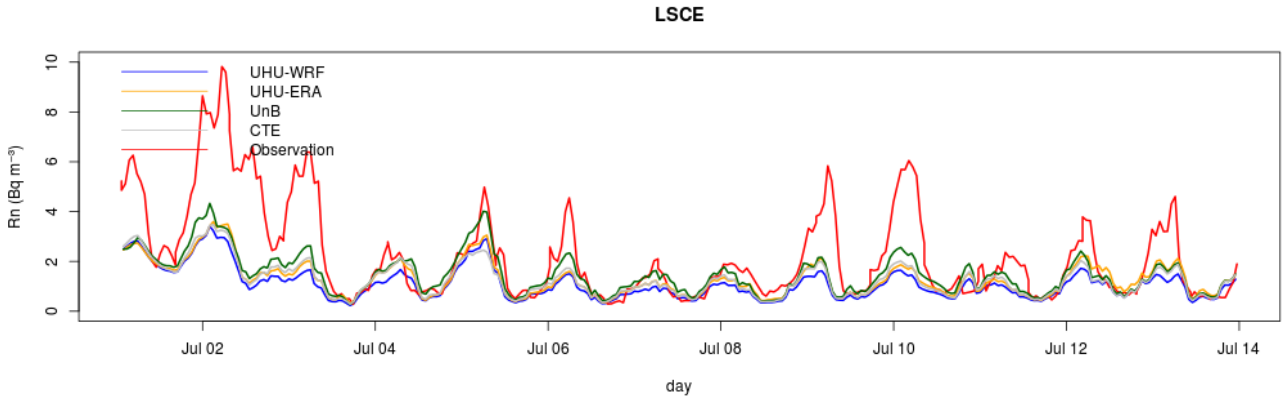

Figure A.3.d) Simulated and observed Radon concentration evolution for LSCE during the period 01/07/2008-14/07/2008

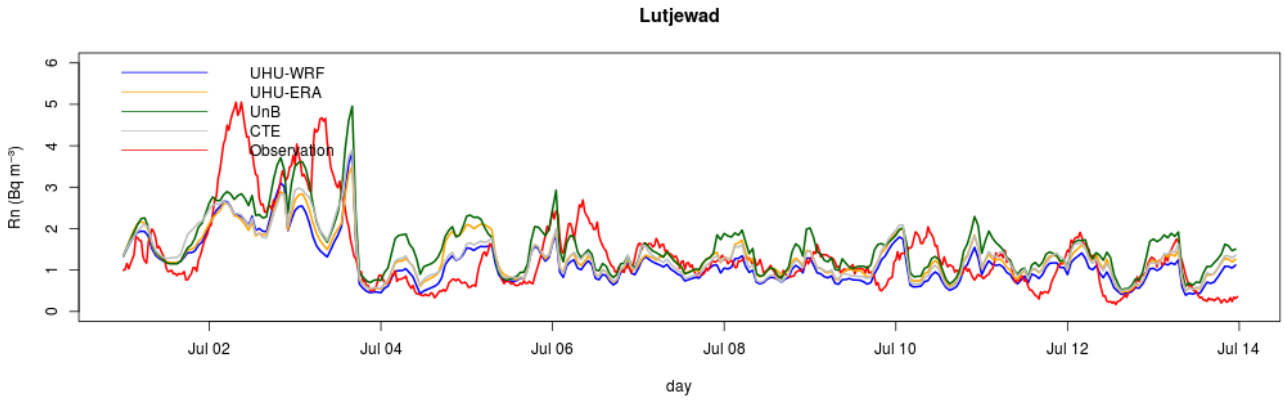

Figure A.3.e) Simulated and observed Radon concentration evolution for Lutjewad during the period 01/07/2008-14/07/2008

A.4 Episode 01/02/2008 - 14/02/2008

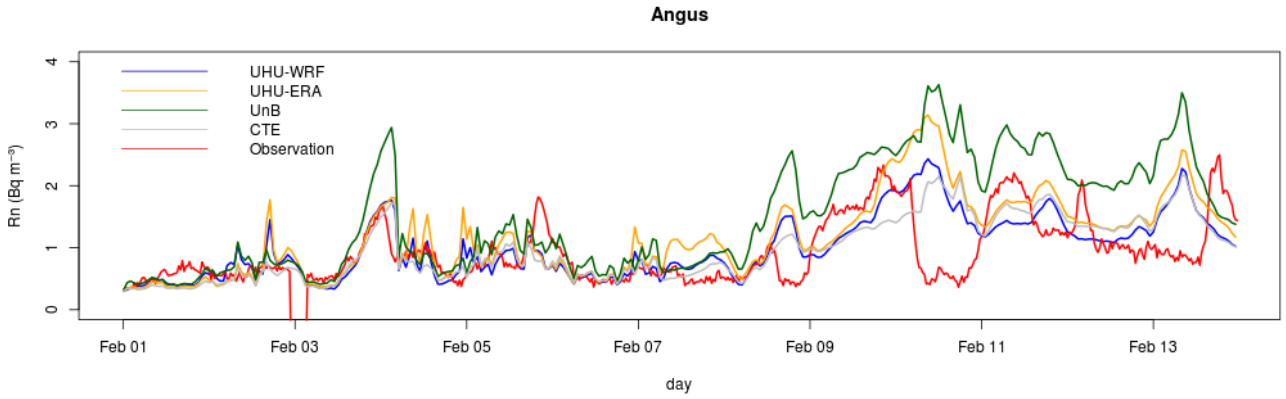

Figure A.4.a) Simulated and observed Radon concentration evolution for Angus during the period 01/02/2008-14/02/2008

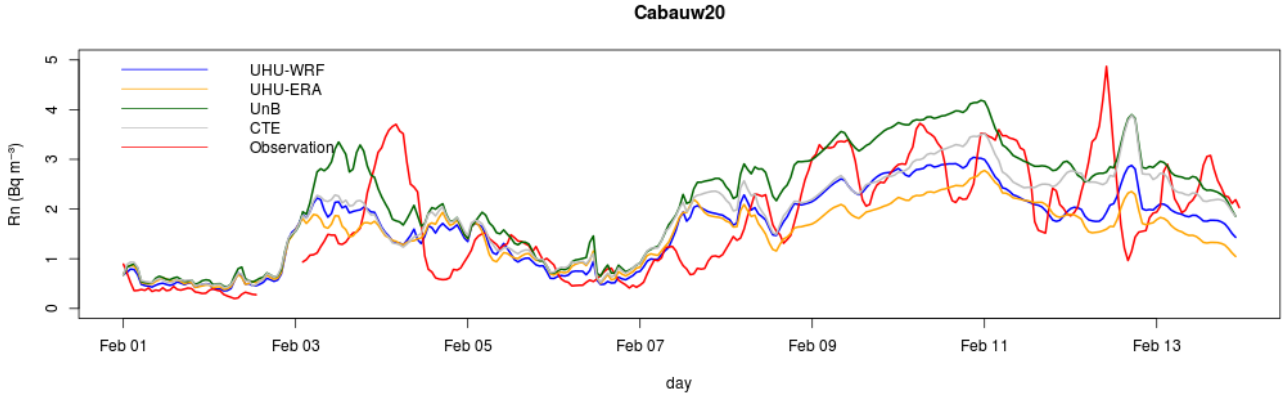

Figure A.4.b) Simulated and observed Radon concentration evolution for Cabauw (20 m) during the period 01/02/2008-14/02/2008

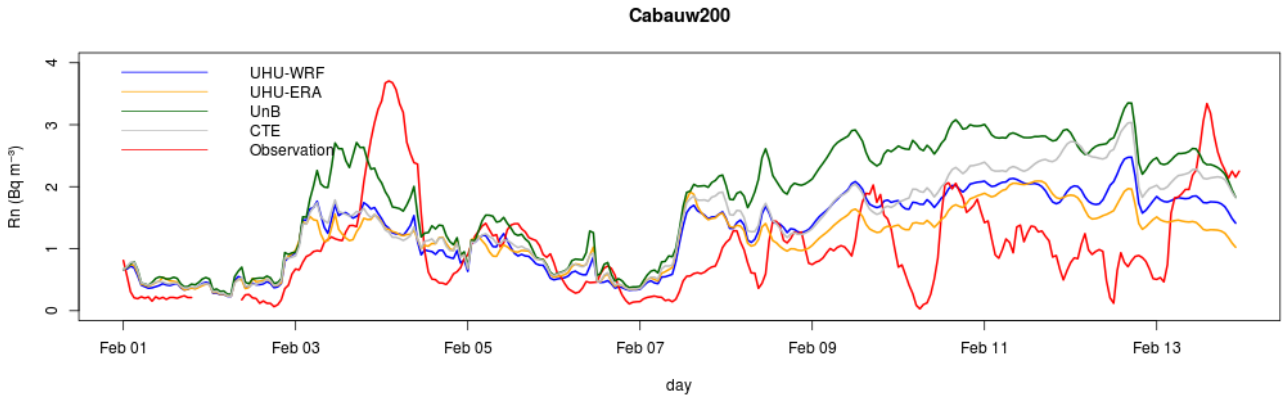

Figure A.4.c) Simulated and observed Radon concentration evolution for Cabauw (200 m) during the period 01/02/2008-14/02/2008

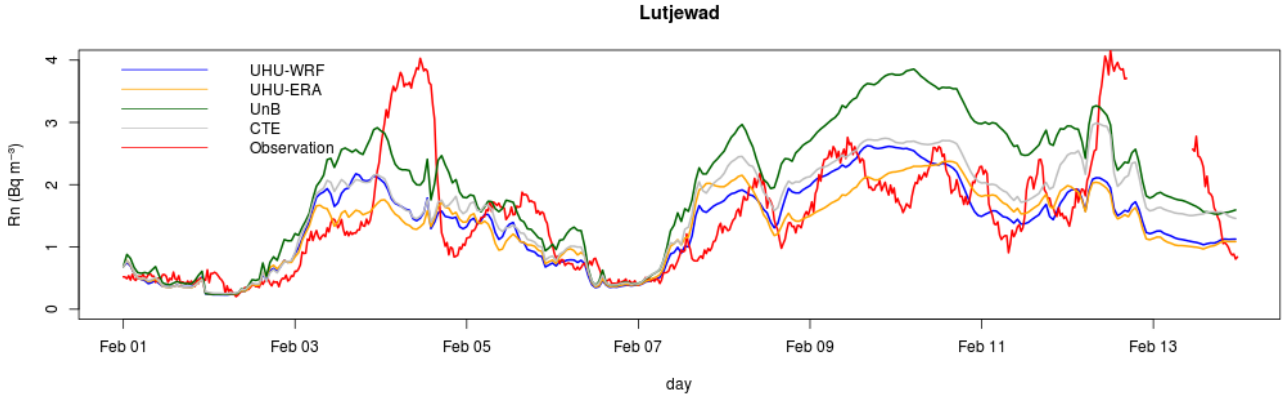

Figure A.4.d) Simulated and observed Radon concentration evolution for Lutjewad during the period 01/02/2008-14/02/2008

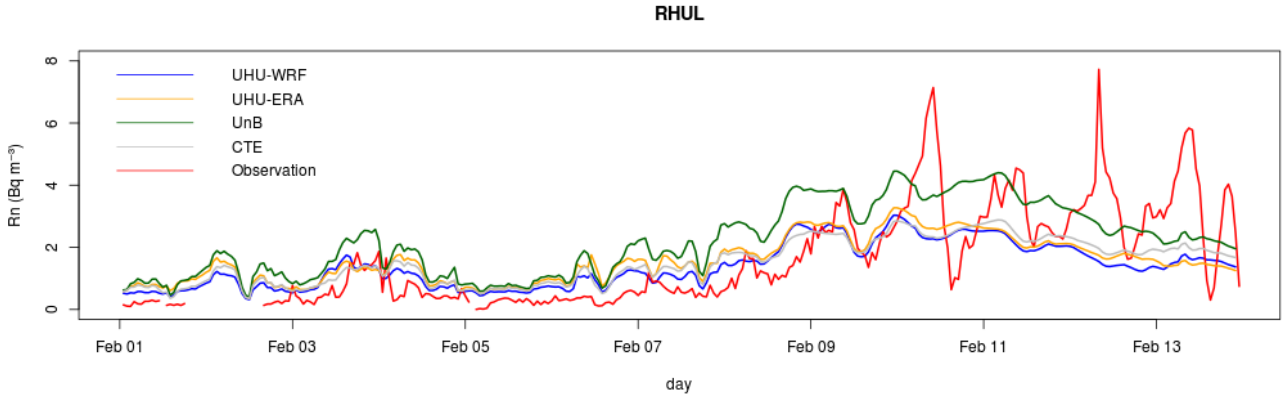

Figure A.4.e) Simulated and observed Radon concentration evolution for RHUL during the period 01/02/2008-14/02/2008

A.5. Episode 01/05/2007 - 14/05/2007

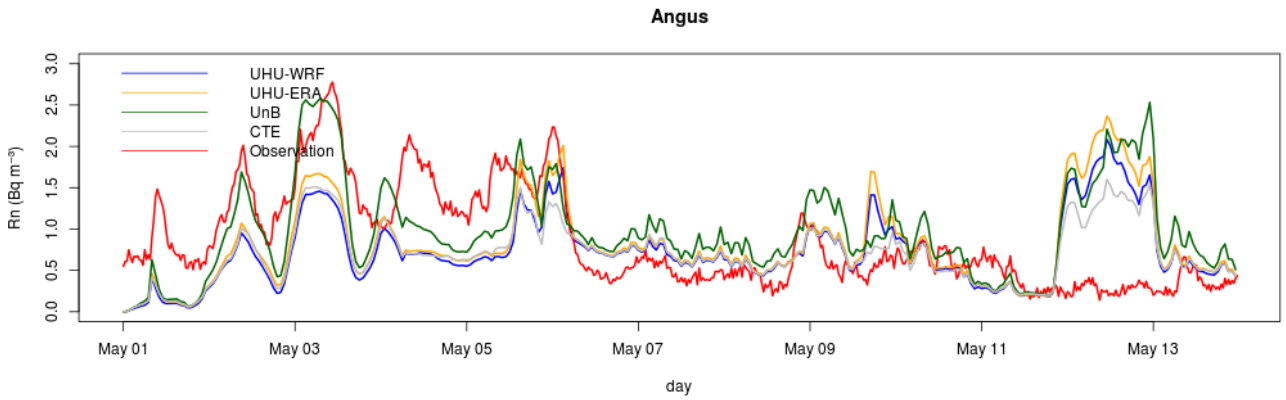

Figure A.5.a) Simulated and observed Radon concentration evolution for Angus during the period 01/05/2007-14/05/2007

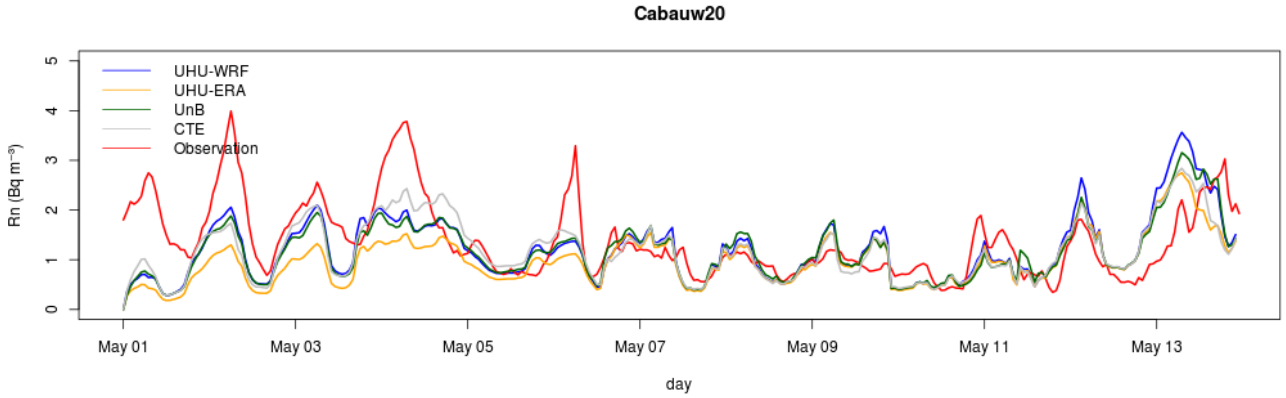

Figure A.5.b) Simulated and observed Radon concentration evolution for Cabauw (20 m) during the period 01/05/2007-14/05/2007

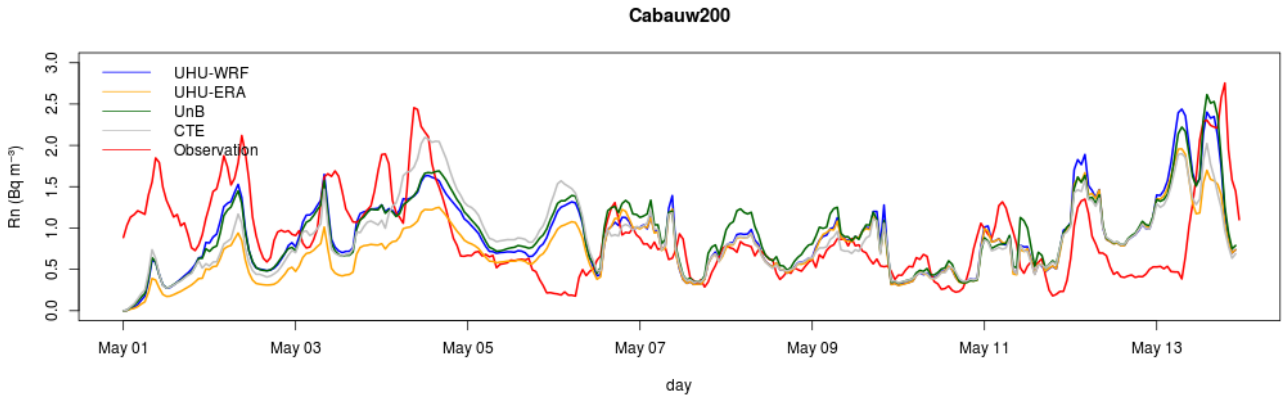

Figure A.5.c) Simulated and observed Radon concentration evolution for Cabauw (200 m) during the period 01/05/2007-14/05/2007

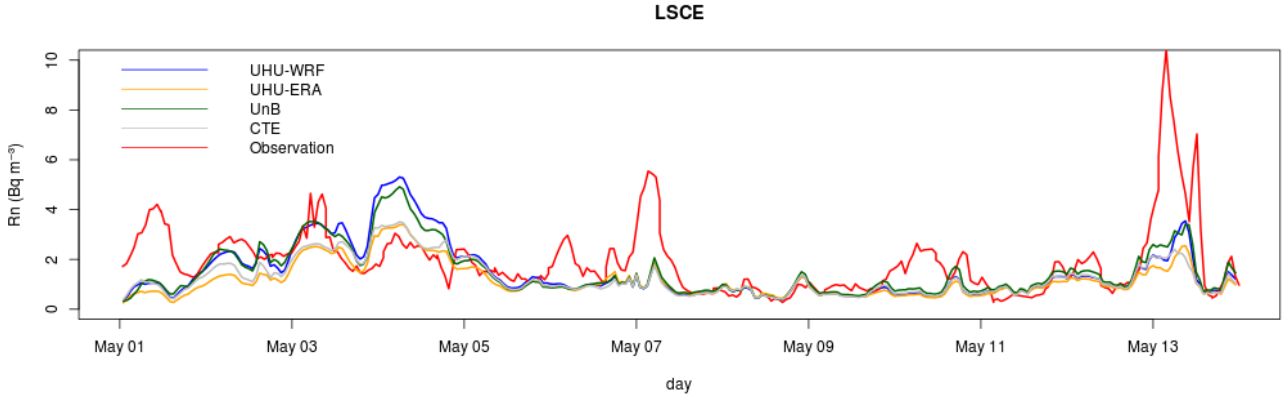

Figure A.5.d) Simulated and observed Radon concentration evolution for LSCE during the period 01/05/2007-14/05/2007

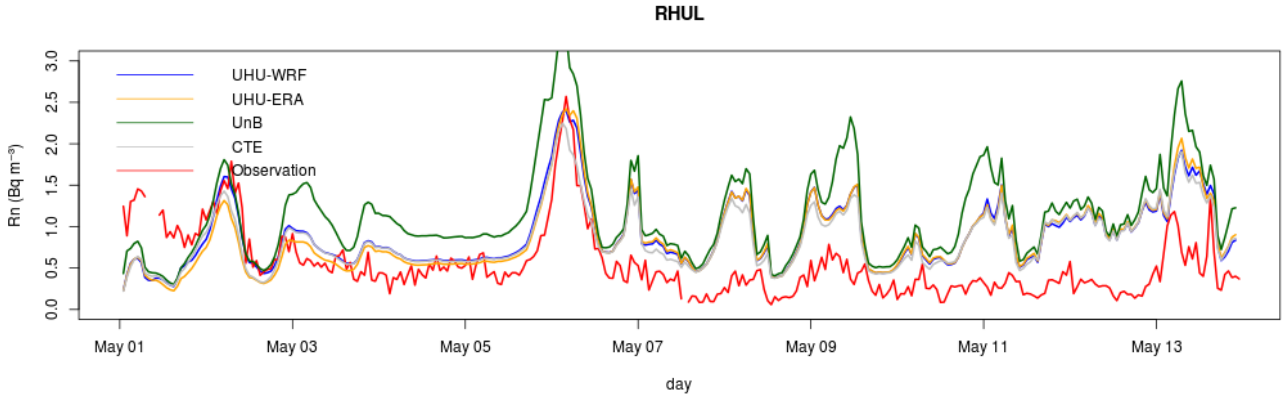

Figure A.5.e) Simulated and observed Radon concentration evolution for RHUL during the period 01/05/2007-14/05/2007